Estimating open water evaporation for the Murray-Darling Basin

A report to the Australian Government from the CSIRO Murray-Darling Basin Sustainable Yields Project

D.L. McJannet, I.T. Webster, M.P. Stenson, B.S. Sherman

November 2008

Murray-Darling Basin Sustainable Yields Project acknowledgments

The Murray-Darling Basin Sustainable Yields project is being undertaken by CSIRO under the Australian Government's Raising National Water Standards Program, administered by the National Water Commission. Important aspects of the work were undertaken by Sinclair Knight Merz; Resource & Environmental Management Pty Ltd; Department of Water and Energy (New South Wales); Department of Natural Resources and Water (Queensland); Murray-Darling Basin Commission; Department of Water, Land and Biodiversity Conservation (South Australia); Bureau of Rural Sciences; Salient Solutions Australia Pty Ltd; eWater Cooperative Research Centre; University of Melbourne; Webb, McKeown and Associates Pty Ltd; and several individual sub-contractors.

Murray-Darling Basin Sustainable Yields Project disclaimers

Acknowledgments

Funding for this work was provided by the National Water Commission. This work would not have been possible without the help of the people who contributed to various areas of data acquisition, data manipulation, interrogation of temporal datasets and analysis of satellite imagery and GIS datasets: Steve Marvanek, Trevor Pickett, Juan-Pablo Guerschman, Jorge Pena Arancibia, Mohammed Mainuddin, Mick Hartcher, Yi Liu, Brendan Farthing, Tim McVicar and Tom Van Neil. Albert van Dijk, and Mac Kirby provided valuable suggestions for implementation and running of the model. Scott Wilkinson and Mike Stewardson provided data and guidance for channel metrics calculations. A review of this report by Albert van Dijk greatly improved the final product.

Citation

McJannet DL, Webster IT, Stenson MP, Sherman BS (2008) Estimating open water evaporation for the Murray Darling Basin. A report to the Australian Government from the CSIRO Murray-Darling Basin Sustainable Yields Project. CSIRO, Australia. 50pp.

Enquires should be addressed to:
David McJannet
david.mcjannet@csiro.au

Publication Details

ISSN 1835-095X

Preface

This is a report to the Australian Government from CSIRO. It is an output of the Murray-Darling Basin Sustainable Yields Project which assessed current and potential future water availability in 18 regions across the Murray-Darling Basin (MDB) considering climate change and other risks to water resources. The project was commissioned following the Murray-Darling Basin Water Summit convened by the then Prime Minister of Australia in November 2006 to report progressively during the latter half of 2007. The reports for each of the 18 regions and for the entire MDB are supported by a series of technical reports detailing the modelling and assessment methods used in the project. This report is one of the supporting technical reports of the project. Project reports can be accessed at http://www.csiro.au/mdbsy.

Project findings are expected to inform the establishment of a new sustainable diversion limit for surface and groundwater in the MDB – one of the responsibilities of a new Murray-Darling Basin Authority in formulating a new Murray-Darling Basin Plan, as required under the Commonwealth Water Act 2007. These reforms are a component of the Australian Government's new national water plan 'Water for our Future'. Amongst other objectives, the national water plan seeks to (i) address over-allocation in the MDB, helping to put it back on a sustainable track, significantly improving the health of rivers and wetlands of the MDB and bringing substantial benefits to irrigators and the community; and (ii) facilitate the modernisation of Australian irrigation, helping to put it on a more sustainable footing against the background of declining water resources.

Executive Summary

This report describes a model developed for estimating evaporation from open water surfaces in the Murray-Darling Basin (MDB). The model was developed as part of the Murray-Darling Basin Sustainable Yields Project which aims to estimate the quantity and temporal variability of water resources across the MDB. A review of the literature and available techniques for estimating evaporation identified 'combination methods' as the most appropriate for estimating evaporation from open water in the MDB based on the available datasets. The combination method used was the Penman-Monteith method with an adjustment to the amount of energy available for evaporation based on changes in heat storage within the water body. Such adjustments are made by estimating the temperature of the water using equilibrium temperature concepts. The model runs on readily available datasets.

The model is tested against measured datasets from seven different locations within the MDB and was shown to produce reliable estimates of the net radiation (difference in average daily values less than 5%), water temperature (difference in average daily values less than 6%), and evaporation (difference in average daily values less than 10%) from water bodies ranging in size from irrigation channels to large reservoirs. An uncertainty analysis demonstrated the sensitivity of evaporation estimates to each input variable and showed that errors are most likely to arise from uncertainty in the estimation of open water area.

It is concluded that the open water evaporation model that we have developed for the MDB is suitable for assessing evaporation from different water bodies of a range of sizes over such a large area. The model runs on readily available datasets and produces reliable results.

Table of Contents

Tables

Figures

1 Introduction

In the light of recent water scarcity and allocation issues in the Murray-Darling Basin (MDB), CSIRO has been contracted by the National Water Commission to report on current and future water availability.

The key goals of this project are to:

- develop a transparent, consistent and robust method for determining the extent of available water resources in each major catchment and aquifer and the MDB as a whole
- apply the method to estimate the quantity and temporal variability of water resources that are available under current water sharing arrangements
- apply the method to estimate water availability and demand 20 years into the future in the light of predicted climate change and other risks.

The Murray-Darling Basin Sustainable Yields Project represents the most comprehensive hydrologic modelling ever attempted for the MDB. It uses rainfall-runoff models, groundwater recharge models, river system models, evaporation models and groundwater models, and considers all upstream–downstream and surface–subsurface connections.

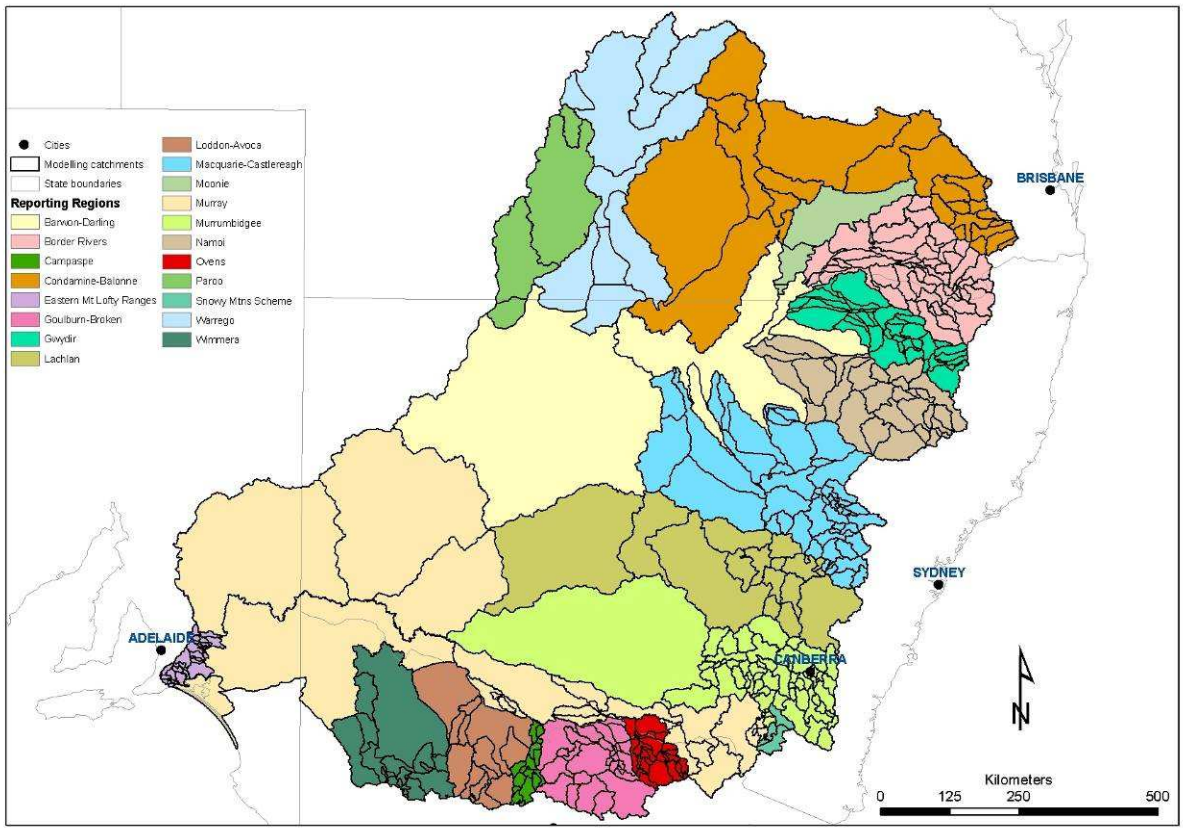

Figure 1-1. The Murray-Darling Basin showing regions, or catchments, and subcatchments

The Murray-Darling Basin Sustainable Yields Project is reporting progressively on each of 18 contiguous regions that comprise the entire MDB. These regions are primarily the drainage basins of the Murray and the Darling rivers – Australia's longest inland rivers, and their tributaries. The regions for which the project assessments are being undertaken and reported are the Paroo, Warrego, Condamine-Balonne, Moonie, Border Rivers, Gwydir, Namoi, Macquarie-Castlereagh, Barwon-Darling, Lachlan, Murrumbidgee, Murray, Ovens, Goulburn-Broken, Campaspe, Loddon-Avoca, Wimmera and Eastern Mount Lofty Ranges (see Figure 1-1). Each of these 18

regions, or catchments, are further divided into reaches and subcatchments. Reaches consist of one or more subcatchments. One of the major aims of the Murray-Darling Basin Sustainable Yields Project is to undertake water accounting for each of the reaches on a monthly time scale. This report describes the development and testing of a methodology for estimating the monthly evaporative losses from open water bodies of all types within each catchment and subcatchment in the MDB.

The development of an approach and framework for estimating open water evaporation losses in the MDB consisted of a number of tasks described in this report including:

- literature review and determination of most suitable technique
- testing of model against available measurements
- compilation of meteorological and geographic datasets to run the model across the MDB
- development and application of a framework for the estimation of evaporative losses from open water bodies across the MDB
- determination of uncertainty in input data and model prediction.

This report also provides background information for catchment-by-catchment reports on water availability which will be published as part of the deliverables to the National Water Commission.

2 A brief review of methods for estimating open water evaporation

A number of publications in the scientific literature compare different methods for estimating open water evaporation rates. One of the most thorough is the review of methods presented by Finch and Hall (2001). This review was undertaken as part of a study for the Environment Agency in the United Kingdom to determine the best means by which to estimate open water evaporation for informing abstraction licences, water balance studies and wetland and still waters management. As such, this review has a similar aim to our aim of estimating open water evaporation in the MDB and the findings of the Finch and Hall report form the basis of the summary below. We first consider the common methods used for estimating evaporation rates.

2.1 Pan factors

Evaporation pans have been used to estimate evaporation rates for many years (see Hounam (1973) for a review). These pans can be of varying dimensions but the most common is the US Class A pan. Pan evaporation is simply the depth of water evaporated from the pan during a day. Some authors have used pan coefficients to relate pan evaporation to observed open water evaporation. There are numerous coefficients reported in the literature but the shortfall of this technique is that coefficients are specific to the pan type, its location and the nature of the water body and so require calibration for individual applications. For larger water bodies pan coefficients may also vary in time to account for heat storage effects. While interpolated daily pan evaporation estimates are available for all of Australia from the SILO database, the uncertainty involved in developing coefficients, particularly given the lack of suitable datasets for calibration, makes this approach unattractive.

2.2 Mass balance

Mass balance techniques calculate evaporation by looking at the differences between storage volume and inflows and outflows for specific water bodies. Some authors report errors of just 5% (e.g. Lapworth, 1965) using such methods. While simple in principle such a method requires detailed and accurate measurements of surface and subsurface flows which are very rarely available. Any errors in estimating components of the mass balance results in a direct error to the evaporation estimate (see Gangopaghaya et al., 1966). The range and number of water bodies in the MDB and the lack of basic mass balance data excludes this method.

2.3 Energy budget

In this method the evaporation from a water body is estimated as the difference between energy inputs and outputs measured at a site. The energy loss through evaporation represents a major component of the energy balance in a typical water body. This method can be accurate if suitable measurements are available (Anderson, 1954; Stewart and Rouse, 1976), but its problem is that specialised equipment is required for each water body if accurate budgets are to be constructed. As with the mass balance approach, any errors in energy balance components are passed through to evaporation estimates directly. The site-specific nature of this method also excludes it from this project.

2.4 Bulk transfer (aerodynamic method)

Evaporation rate (E) can also be estimated using the application of bulk transfer formulae. A simple version of such a bulk transfer equation is shown in Equation 1 (Dalton, 1802):

$$E = CU(e_s^* - e) \qquad \text{Equation 1}$$

where C is a mass transfer coefficient, U is wind speed and $(e_s^* - e)$ is the difference between saturated vapour pressure at the temperature of the water surface and the vapour pressure at a specified height in the air above the water surface. The mass transfer coefficient is similar in concept to a drag coefficient implicitly incorporating transfer across the viscous skin layer at the water surface and through the turbulent flow above it. Numerous studies have shown that the coefficient changes at wind speeds corresponding to the onset of capillary wave formation on the water surface. As well, the coefficient depends on the stability of the atmosphere (Liu et al., 1979). The coefficient may also vary depending on fetch across the water surface and vegetation of the surrounding land. This method requires measurements of wind speed, vapour pressure, and air and water surface temperature, as well as estimates or measurements of water temperature. While not all of these variables are readily available for the MDB, techniques exist by which to estimate them. Bulk transfer techniques are best suited to larger water bodies with fetches of at least several hundred metres. Hence these techniques have limited applicability to the size and range of water bodies for which evaporation rate needs to be modelled in the MDB.

2.5 Combination methods

The so-called ‘combination methods’ combine the mass transfer and energy budget principles in a single equation. Two of the most commonly known combination methods are the Penman equation (Penman, 1948) and the Penman-Monteith equation (Monteith, 1965). The combination equations require inputs of net radiation, air temperature, vapour pressure and wind speed. Air temperature and vapour pressure data have been interpolated for all locations in Australia, as has solar radiation which can be used to estimate net radiation (see below). This data – in combination with wind speed data from widespread Bureau of Meteorology (BoM) gauges – makes the application of combination models at any location in the MDB possible.

When applied to open water evaporation, the Penman-Monteith approach allows adjustment to the amount of energy available for evaporation based on changes in heat storage within the water body. Such an adjustment can be obtained if the temperature of the water body is known or can be estimated. Useful models by which to determine water temperature have been developed and most are based on the concept of an equilibrium temperature (e.g. de Bruin, 1982; Edinger et al., 1968; Keijman and Koopmans, 1973). Such models utilise the same meteorological driving data as the Penman-Monteith model and indeed the loss of heat through evaporation is an important part of the energy calculation used to calculate temperature. The equilibrium temperature is defined as the surface temperature at which the net rate of heat exchange would be zero.

Shallow water bodies may be in temperature equilibrium with their meteorological forcing, but deeper water bodies may store sufficient heat in the water column that they are not in thermal equilibrium and the surface temperature is greater than or less than the equilibrium temperature. A modification of the equilibrium temperature method allows for this factor to be taken into account in the determination of surface temperature and hence evaporation rate.

2.6 Summary

For the purposes of open water evaporation estimation in the MDB the Penman-Monteith model, with an inclusion for water body heat storage, is considered to be most suitable. The key factors making this technique most appropriate are that:

- calculations are based on readily available data sources
- the model has limited empirical basis and therefore it is more readily applicable to a variety of water bodies
- the model takes into account heat storage within water bodies.

While bulk transfer methods could also have been applied to the MDB we have chosen to use the Penman-Monteith model for consistency across the range of terrestrial and aquatic systems being modelled in the broader Murray-Darling Basin Sustainable Yields Project. The key assumption of the Penman-Monteith model with adjustments for heat storage is that the water body is well mixed and that no thermal stratification develops. The remainder of this report will focus on its implementation, testing and application.

3 Model algorithms

The following section describes the key algorithms used in the open water evaporation model. A full list of symbols and units is given in Appendix 1 and the complete set of algorithms is presented in Appendix 2.

3.1 Key algorithms

The algorithm which is central to the evaporation model to be employed for this project is the Penman-Monteith equation (Monteith, 1965) (Equation 2). This equation can be used to produce a time series of evaporation rate (E in mm d^{-1}) from a water body based on prescribed water surface temperature, air temperature, wind speed and vapour pressure.

$$E = \frac{1}{\lambda}\left(\frac{\Delta_w (Q^* - N) + 86400\rho_a C_a (e_w^* - e_a)/r_a}{\Delta_w + \gamma}\right) \qquad \text{Equation 2}$$

where:

λ (MJ kg^{-1}) is the latent heat of vaporisation,

Δ_w (kPa ℃ $^{-1}$) is the slope of the temperature saturation water vapour curve at water temperature,

Q^* (MJ m^{-2} d^{-1}) is net radiation,

N (MJ m^{-2} d^{-1}) is change in heat storage in the water body,

ρ_a (kg m^{-3}) is density of air,

C_a (MJ kg^{-1} ^{o}K^{-1}) is specific heat of air,

e_w^* (kPa) is saturated vapour pressure at water temperature,

e_a (kPa) is vapour pressure at air temperature,

r_a (s m^{-1}) is aerodynamic resistance, and

γ (kPa ℃ $^{-1}$) is the psychometric constant.

The change in heat storage of the water body, *N*, is central to the open water evaporation model as it affects water surface temperatures and, hence, evaporation. The depth of a water body affects its potential to store energy; therefore, our model needs to be able to predict changes in this heat store over time. Within the model, changes to water temperature and heat storage are reliant on the equilibrium temperature (T_e) and the time constant (τ). The equilibrium temperature is defined as the surface temperature at which the net rate of heat exchange would be zero, while the time constant controls changes in water temperature and is based largely on the depth of the water column.

Water temperature, T_w (℃), is calculated from Equation 3 (de Bruin, 1982):

$$T_w = T_e + (T_{w0} - T_e)\exp(-1/\tau) \qquad \text{Equation 3}$$

The equilibrium temperature, T_e (℃), is calculated from Equation 4 (de Bruin, 1982) :

$$T_e = T_n + \frac{Q^*_n}{4\sigma(T_n + 273.15)^3 + f(u)(\Delta_n + \gamma)} \qquad \text{Equation 4}$$

where:

T_n (℃) is the wet-bulb temperature,

Q^*_n (MJ m^{-2} d^{-1}) is the net radiation at wet-bulb temperature,
σ (MJ m^{-2} $^oK^{-4}$ d^{-1}) is the Stefan-Boltzmann constant,
$f(u)$ (MJ m^{-2} d^{-1} kPa^{-1}) is the wind function (Equation 6), and
Δ_n (kPa ℃ $^{-1}$) is the slope of the temperature saturation water vapour curve at air temperature.

The time constant, τ , in days is calculated using Equation 5 (de Bruin, 1982):

$$\tau = \frac{\rho_w C_w Z}{4\sigma(T_n + 273.15)^3 + f(u)(\Delta_n + \gamma)} \qquad \text{Equation 5}$$

where:
ρ_w (kg m^{-3}) is the density of water,
C_w (MJ kg^{-1} $^oK^{-1}$) is the specific heat of water, and
Z (m) is the depth of water.

The wind function, *f(u)*, is used in heat budget studies to define the evaporation rate from which latent heat loss is calculated. Studies from a number of different sized water bodies suggest that the evaporation coefficient should be not only a function of wind speed, but also of water body size. It seems that water body size affects the aerodynamic resistance to evaporative mass transfer. As air flows from the land to over the water, the surface roughness reduces abruptly. The turbulence in the air flow gradually adjusts itself to this change at increasing distances from the shore. Further, as water is being gradually evaporated into the air flow, the humidity of the air increases downwind from the shore. Both of these effects, which mostly act in opposite directions to one another, tend to cause variation in evaporation rate over the water surface and so with water body size (area). In the analysis of evaporation from different sized water bodies in the MDB, incorporation of the influence of water body area is seen as essential because of the wide range of water bodies being studied. We have chosen the wind function of Sweers (1976) which is a further development of the work of McMillan (1973) at a 5 km^2 lake in Wales which has been modified to include effects of water body area based on the methods developed by Harbeck et al. (1962). Sweers presents wind functions from McMillan's work for wind, air temperature and humidity measurements taken over land and over water. We will employ the wind function adjusted for area based on measurements taken over land:

$$f(u) = \left(\frac{5}{A}\right)^{0.05} (3.80 + 1.57U_{10}) \qquad \text{Equation 6}$$

where:
U_{10} (m s^{-1}) is the wind speed at 10 m height, and
A (km^2) is the area of the water body (note that the square of the width is used for elongated water bodies).

Full description of all equations used in the model are given in Appendix 2 and the model framework is described in Appendix 3. The data requirements for calculating daily evaporation rate are:

- mean daily air temperature
- mean daily wind speed
- total daily solar radiation
- vapour pressure
- water body depth
- water body area
- water body altitude (used in the estimation of clear sky solar radiation inputs at a location)
- water body latitude (used in the estimation of extraterrestrial solar radiation inputs).

4 Data inputs

4.1 Time series inputs

The time series data in Table 4-1 are used as inputs to the open water evaporation model.

Table 4-1. Time series data inputs

Data	Symbol	Units
Date of data	D	dd/mm/yyyy
Mean daily air temperature	T_a	℃
Daily vapour pressure (taken as 9:00 am)	e_a	kPa
Total daily incoming short-wave radiation	$K\downarrow$	MJ m^{-2} d^{-1}
Average daily wind speed at 10 m	U_{10}	m s^{-1}

The primary source of meteorological data is the SILO database which can be found at http://www.nrw.qld.gov.au/silo/. The SILO database consists of interpolated meteorological variables on a 0.05°(5 km) grid for the whole of Australia (Jeffrey et al., 2001). The particular variables available from SILO used by the equilibrium evaporation model are air temperature, vapour pressure and solar radiation. For evaporation modelling all SILO 0.05°grid point datasets within each subcatchment are identified and collated. The daily data is then averaged across all sites to produce a subcatchment average of air temperature, vapour pressure and solar radiation. Standard deviations of all variables are also calculated for assessment of potential error in evaporation calculations. It may be possible to run the model for individual water bodies based on climate and wind speed data from the nearest location, but this is much more computationally complex and involves tracking each individual water body over time – beyond the scope of this project.

Wind speed data for each pixel in the MDB was determined from the interpolated dataset of McVicar et al. (*In prep.*). Unlike the SILO database the wind speed data is point specific; therefore, a subcatchment averaging process needed to be undertaken. Using the subcatchment boundaries defined for this project, the wind speed stations in each subcatchment were identified and the data extracted.

4.2 Water body and site characteristics

The model application requires the specification of the water body and site characteristics listed in Table 4-2.

Table 4-2. Site characteristics data input

Data	Symbol	Units
Water body depth	Z	m
Water body altitude	ψ	m
Latitude	φ	radians
Water body area	A	km^2

4.2.1 Water body characteristics

In order to convert evaporation rate data for different water bodies to evaporation volume it was necessary to estimate the area of each water body type in a catchment. Water body types included irrigation channels (channels, drains and aqueducts), reservoirs, ponds, streams, lakes and areas inundated by floods.

Due to a lack of better datasets, all water body types except streams and flood areas were considered to be constant in time, but we recognise that seasonal changes in water depths (and areas) may be significant. Values for the area (or length) of each of these water body types were extracted from the GEODATA TOPO 250K Series 3 Topographic Data set from Geosciences Australia (see Kirby et al, 2008). Water body width and depth were estimated differently for irrigation channels, streams, lakes, reservoirs and flooded areas.

For irrigation channels, recognising that width will influence evaporation rate, we define three size classes: channels 1 m wide, channels 2 to 10 m wide, and channels >10 m wide. The length of each of these channel classes were then estimated based on an analysis of channel widths from satellite imagery and analysis of the channel width distributions within these classes (see Kirby et al, 2008).

Although stream length information exists there is no stream width information available for computing areas. In the field of channel metrics, relationships are commonly developed between channel width (L), channel depth (D) and discharge (Q) (e.g. Leopold and Maddock, 1953; Leopold et al., 1964). Therefore, it is possible to use such relationships to estimate stream widths. Details of the techniques used to determine average stream width are given in Kirby et al. (2008).

Areas inundated by flooding were determined by analysis of MODIS satellite images (see Kirby et al, 2008). When flooding occurred the area of stream in each subcatchment was subtracted from the total area to avoid double counting.

Characteristics of the different water bodies used in the MDB open water evaporation modelling are shown in Table 4-3. Following the methodology of Sweers (1976) the area of elongated narrow water bodies is defined by the width (in km) squared. In each subcatchment the model is used to calculate evaporation rate (mm d^{-1}) for each of these water body types using the fixed values in Table 4-3. Justification of the use of fixed values is given in Section 6. Estimates of actual evaporation volume will depend on actual areas of water bodies determined for each subcatchment.

Table 4-3. Water body characteristics used for evaporation modelling

Water body type	Depth	Area	Width
Irrigation channel 1	0.75 m	-	1
Irrigation channel 2	2.0 m	-	4.5
Irrigation channel 3	3.0 m	-	14.5
Pond	3.0 m	0.01 km^2	-
Lake	4.0 m	0.5 km^2	-
Reservoir	7.0 m	4.0 km^2	-
Stream	4.0 m	-	Dynamic
Floodplain	1.0 m	Dynamic	-

4.2.2 Site characteristics

The site characteristics required for the evaporation model are altitude and latitude. This information was extracted for each catchment using GIS analysis of the MDB digital elevation model and catchment boundary information. For each subcatchment the average altitude and latitude was determined. The standard deviation of these values was also determined for uncertainty analysis (see Section 6).

5 Model performance

The locations of field sites where data was available for testing evaporation model predictions are shown in Figure 5-1. Test water bodies ranged from large-scale dams and lakes to irrigation channels. Details of the data sites and datasets are given below. Each dataset was tested by running the model as it would be in the modelling framework. The subcatchment where the test site was located was determined and the associated average subcatchment elevation, latitude, and average SILO and wind speed datasets were used as specified in the model description above.

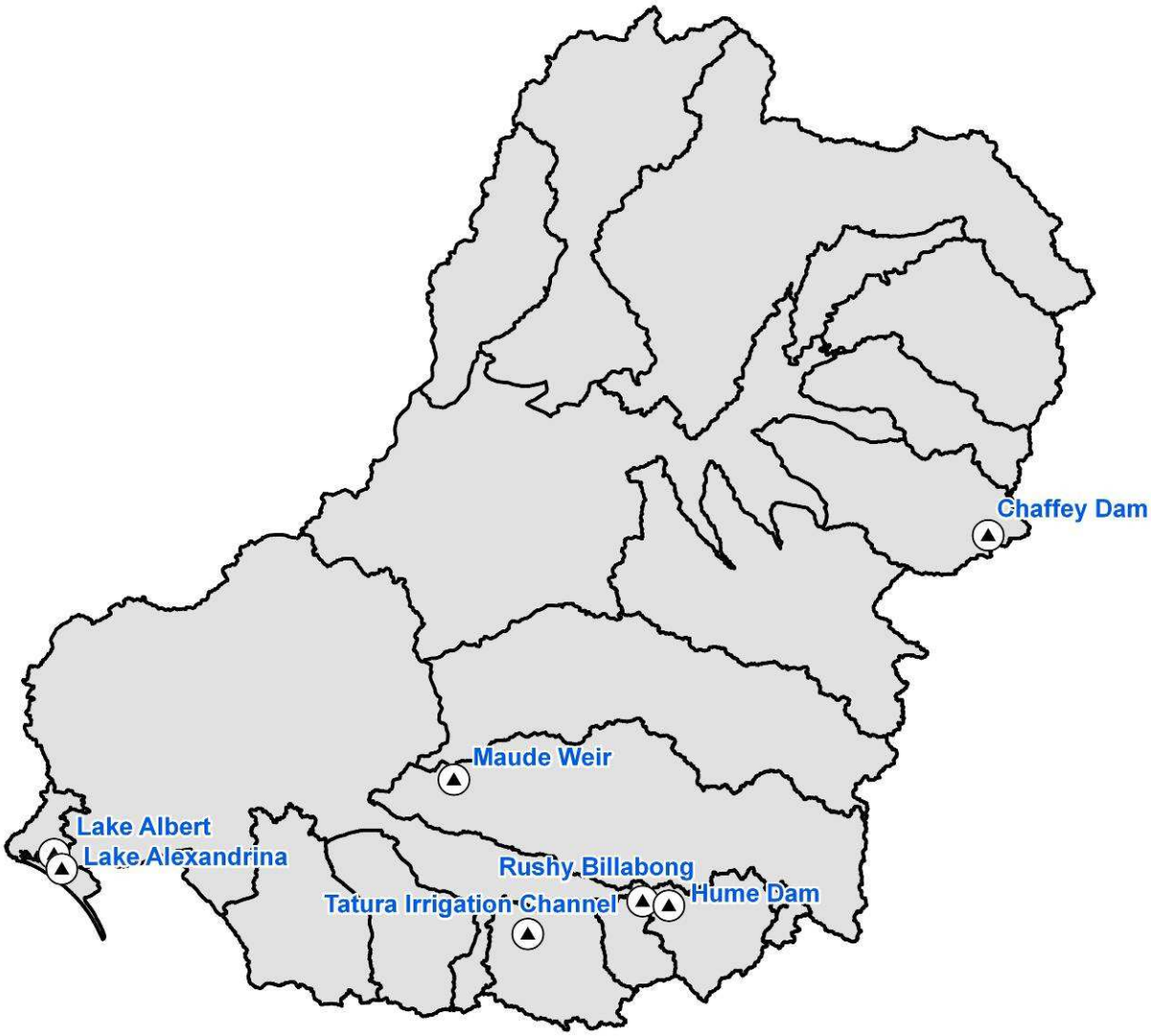

Figure 5-1. Locations of sites with test data in the Murray-Darling Basin

We assess the ability of the model not only to predict evaporation rates measured at each site but also to assess the performance of the model in predicting the processes which drive evaporation (i.e. water temperature, net radiation, wind speed). Such an analysis identifies where the sources of error arise in the evaporation estimates. For all studies, except some of the older studies from Lake Alexandrina and Lake Albert, the climate data used to run the model is a subcatchment average of available SILO data points and wind speed is an average of that interpolated for each pixel in the subcatchment. In this way the model is being tested in the same way in which it will be run for the MDB. For the pre-1990 studies from Lake Alexandrina and Lake Albert, climate and wind speed data are taken from the nearest BoM station.

A common method for estimating evaporation from open water is to use evaporation pan data and a scaling factor. A commonly used scaling factor is a multiplier of 0.7 (e.g. Khan et al., 2004; Stanhill, 1976). A key question then is: how much better are evaporation estimates likely to be by using the evaporation model described in this report rather than just applying a pan factor? To explore this further, where applicable, we compare measured and modelled evaporation with scaled evaporation pan data at each site. Evaporation pan data are taken from the SILO database for the nearest 0.05° grid point to th e study site.

5.1 Rushy Billabong

5.1.1 Site characteristics

Rushy Billabong is a small water body (~0.5 km^2) located on the Murray River floodplain 20 km to the west of Albury. This site was the location for an evaporation study by Webster and Sherman (1995). Table 5-1 shows the characteristics of the Rushy Billabong site and the measurements available for model testing. Figure 5-2 shows a satellite image of this location from Google Earth 2007. Rushy Billabong falls within the Murray region of the MDB.

Table 5-1. Site characteristics for Rushy Billabong

Water body location	36° 1'54.06"S, 146°43'0.19"E
Water body area	0.05 km^2
Average water body depth	1.0 m
Measurement period	October 1991 to April 1992
Measurements	Wind speed Net radiation Water temperature Air temperature Specific humidity Evaporation
Evaporation estimation technique	Heat budget
Reference	Webster and Sherman (1995)

Figure 5-2. Satellite image of Rushy Billabong at very low water level. Approximate full Billabong area indicated by yellow line

5.1.2 Results

Figure 5-3 shows a comparison of measured and predicted water surface temperature for Rushy Billabong. The model predictions capture the major variations in measured temperature although they were usually slightly higher than those measured and also did not fall as sharply as those measured. Average modelled temperature (25.5℃) was slightly higher than average measured temperature (24.0℃).

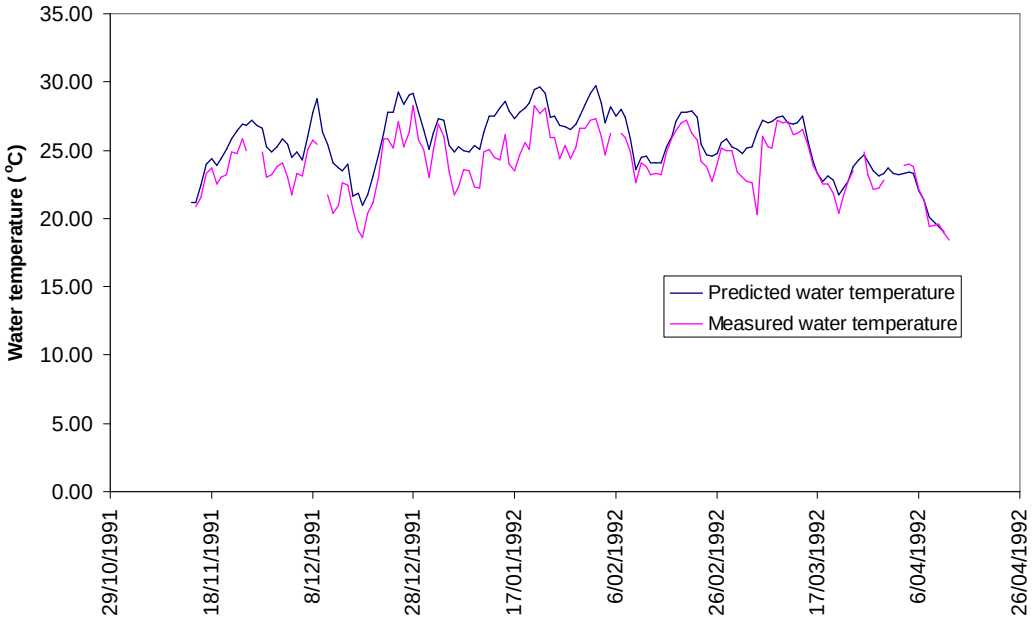

Figure 5-3. Measured and predicted water temperatures at Rushy Billabong

Figure 5-4 shows predicted and measured net radiation at Rushy Billabong. Net radiation predictions are very good and give a great deal of confidence in the methodology used for estimating net radiation from SILO data. Average net radiation from the model was 14.3 Wm^{-2} while averaged measured net radiation was 13.9 Wm^{-2}.

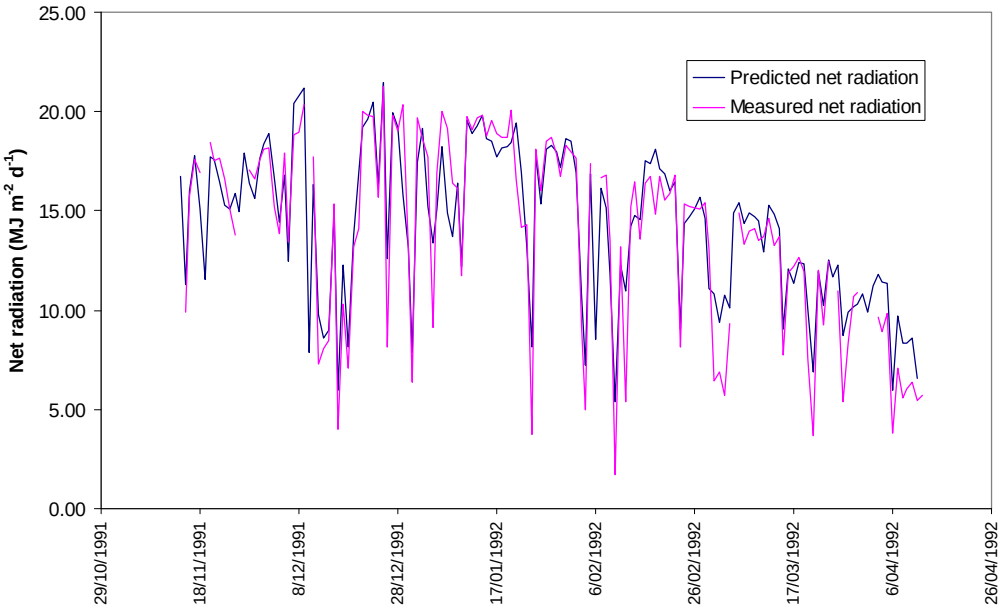

Figure 5-4. Measured and predicted net radiation at Rushy Billabong

Figure 5-5 shows a comparison of measured and predicted daily evaporation rate. The peaks of evaporation are very similar; however, the modelled evaporation does not drop as low as that measured. This observation could be a result of site-specific characteristics, such as wind direction and wind breaks, that we are unable to account for in the model. The model predicted 812 mm of evaporation for the study period while the measurements showed that there was 736 mm – an overestimate of about 10%. Daily average evaporation was 5.9 mm d^{-1} and 5.3 mm d^{-1} for predictions and measurements, respectively. Average measured wind speed was 0.5 m s^{-1} greater than that from the wind speed interpolation. Therefore, if measured wind speed was used in the model, daily average evaporation was 6.2 mm d^{-1}.

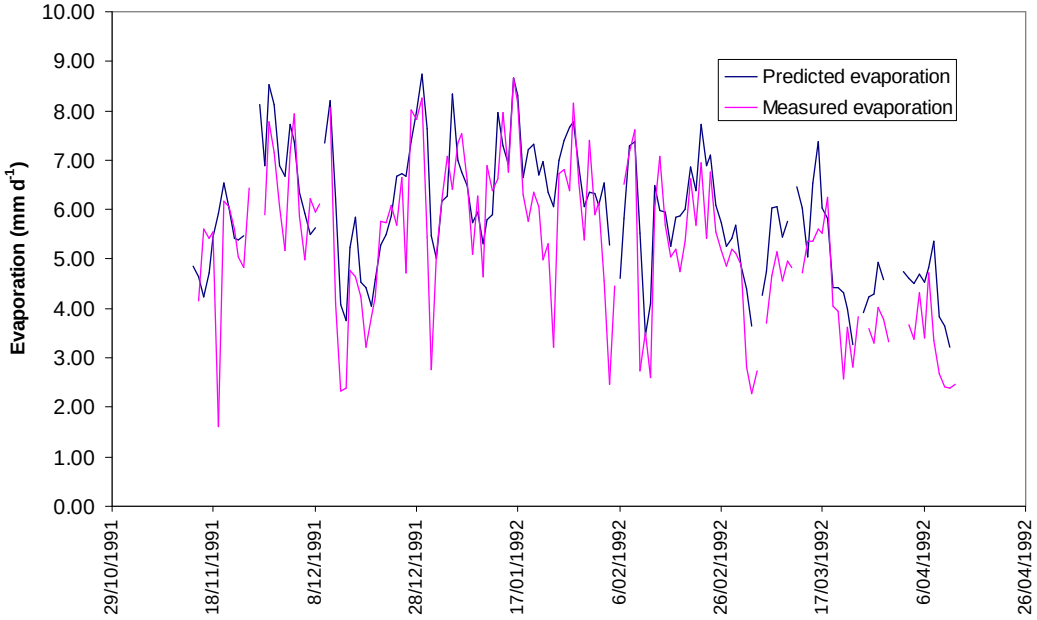

Figure 5-5. Measured and predicted evaporation at Rushy Billabong

The comparison of the evaporation model with measurements is summarised in Table 5-2 which includes average daily and monthly measured and modelled water temperature, net radiation and evaporation. Also shown are the standard error of estimates (SEE) and regression coefficient (r^2) for comparison pairs. The bottom row of the table shows a comparison of scaled pan evaporation (pan coefficient = 0.7) with measured evaporation. This table shows that scaled pan evaporation is about 10% below that measured (compared to a 10% overestimate by the evaporation model) but also that the daily data are less well correlated (r^2 = 0.59) with measurements that the evaporation model estimates (r^2=0.70).

Table 5-2. Daily and monthly measured and modelled results for Rushy Billabong. Also included for reference are measured and modelled scaled pan evaporation

	Average daily measured	Average daily modelled	% Difference	SEE daily	r^2 daily	SEE monthly	r^2 monthly
Water temperature (℃)	24.0	25.5	6%	1.32	0.75	0.61	0.97
Net radiation (MJ m^{-2} d^{-1})	13.9	14.3	3%	1.24	0.78	0.40	0.99
Evaporation (mm)	5.3	5.9	10%	0.92	0.70	0.25	0.97
Scaled pan evaporation (mm)	5.3	4.8	-10%	1.01	0.59	0.19	0.97

SEE – Standard Error of Estimation

5.2 Hume Dam

5.2.1 Site characteristics

Hume Dam, Australia's seventh largest reservoir, is located on the River Murray, 16 km upstream of Albury–Wodonga. When full Hume dam holds 3,057 GL. Serving as the primary regulating dam for irrigation in the MDB and the supply of water to Adelaide, it historically has received a mean annual inflow of 5,970 GL and delivered a mean annual outflow of 5,450 GL (Sherman, 2005). During spring and summer much of the inflow (up to 10,000 ML d^{-1}) is unnaturally cold water (12 to 14 ℃) released from Dartmouth Dam located upstream on the Mitta Mitta River. When full, 1 mm of evaporation is equivalent to about 1.4% of the daily flow through the storage. Full details of the site are given in Table 5-3. Figure 5-6 shows a satellite image of this location from Google Earth 2007. Hume Dam falls within the Murray region of the MDB.

Table 5-3. Site characteristics for Hume Dam

Water body location	36°5'24.13"S, 147°3'9.55"E
Water body area	202.4 km^2
Average water body depth	25.1 m
Measurement period	November 2001 to May 2003
Measurements	Long-wave radiation Wind speed Net radiation Water temperature Air temperature Evaporation
Evaporation estimation technique	Stability corrected bulk formula (Liu et al., 1979)
Reference	Sherman (2005)

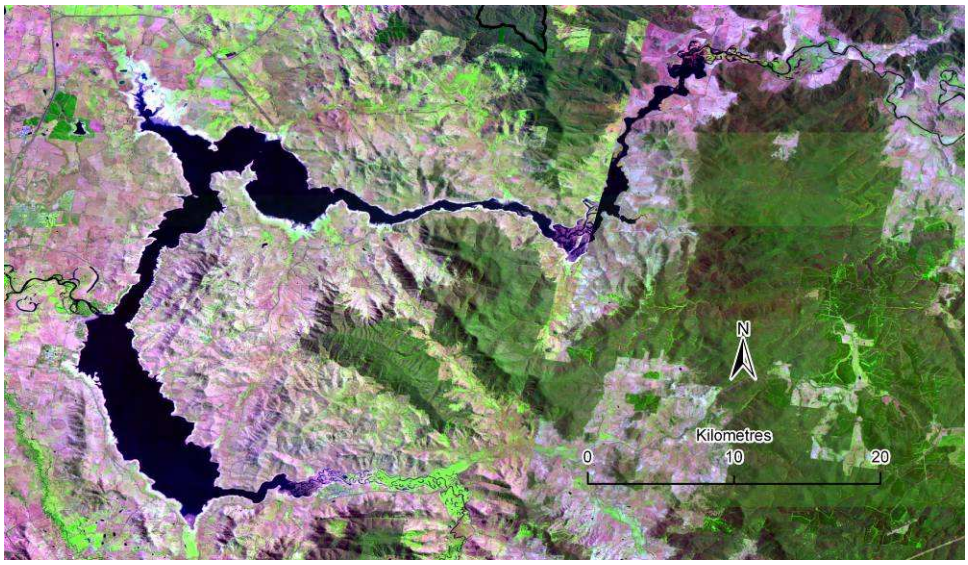

Figure 5-6. Satellite image of Hume dam

5.2.2 Results

Evaporation monitoring at Hume Dam was undertaken by Sherman as part of a report for the Murray-Darling Basin Commission (Sherman, 2005). The dataset from Hume Dam includes measurements of long- and short-wave radiation and water temperature and evaporation which can all be used to test the model. Figure 5-7 shows very close agreement between observed and predicted downwelling long-wave radiation showing that the model is performing very well in estimating this energy input. Figure 5-8 shows a comparison of downwelling solar radiation from the SILO dataset and the Sherman dataset; again the agreement between the two dataset is very good. Average for the SILO dataset is 21.7 MJ m^{-2} d^{-1} while the measured average solar radiation was 22.3 MJ m^{-2} d^{-1}.

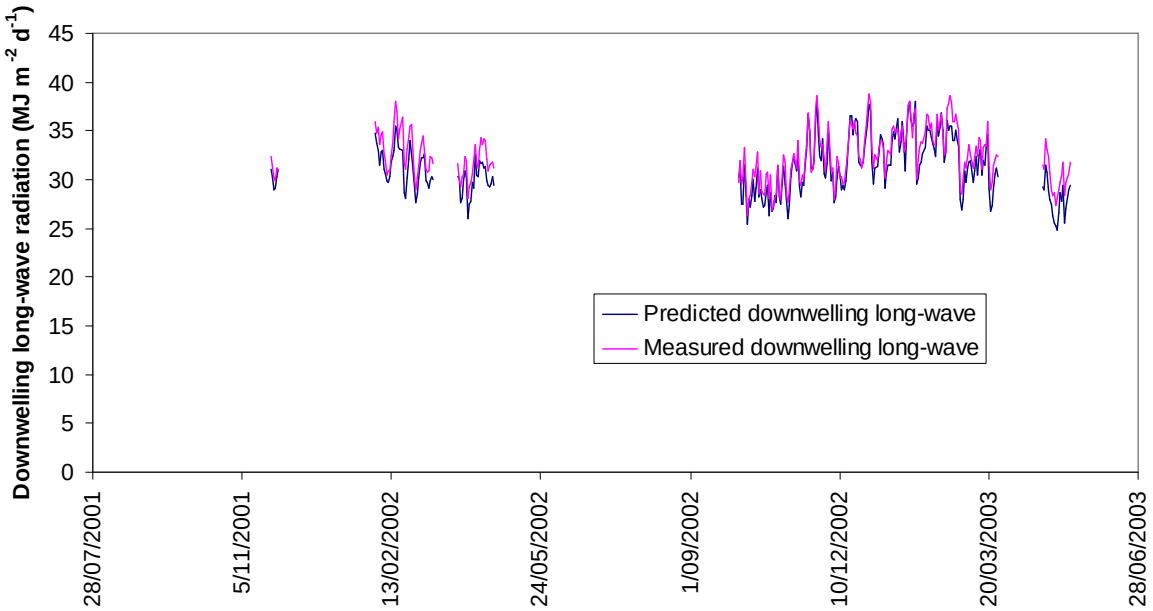

Figure 5-7. Measured and predicted downwelling long-wave radiation at Hume Dam

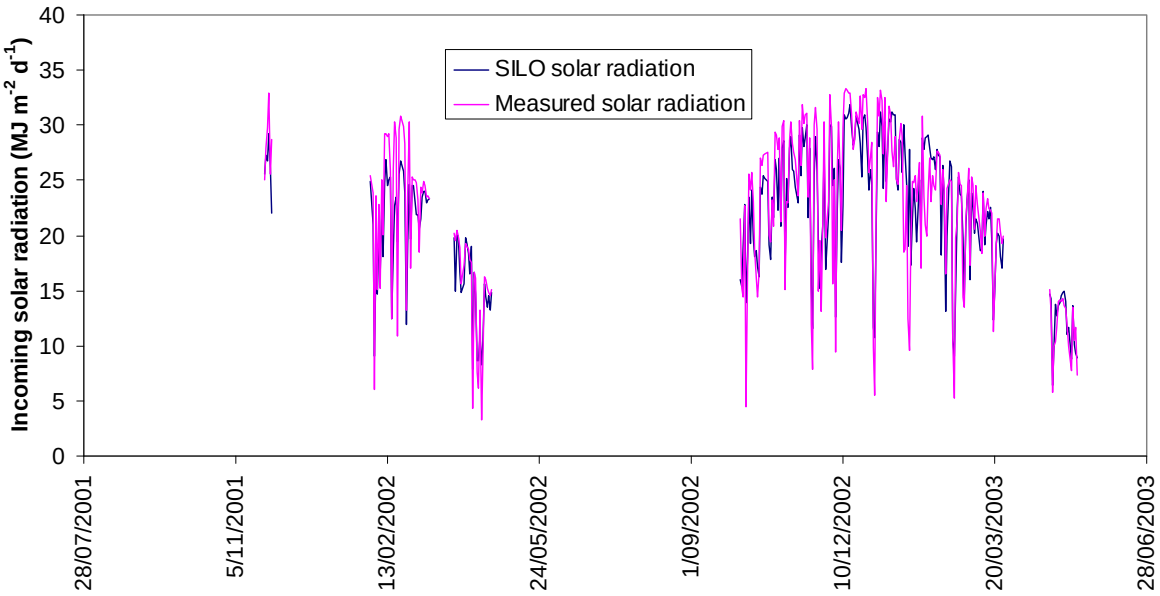

Figure 5-8. Measured and SILO solar radiation at Hume Dam

Despite the good agreement between model and measured incoming radiation, agreement between observed and predicted water temperature is very poor, particularly in the middle of summer (Figure 5-9). This is due largely to an error in estimated wind speed (see below), which is approximately one-half the measured wind speed at the dam. With the short-wave radiative energy inputs roughly correct, another way that such a difference in temperatures is possible is if the dam is receiving cold water inputs. In the case of the Hume Dam, the cold water inputs come in the form of snow melt from the Snowy Mountains. The model employed for this project assumes that there are no external inputs to the water body and hence prediction is poor.

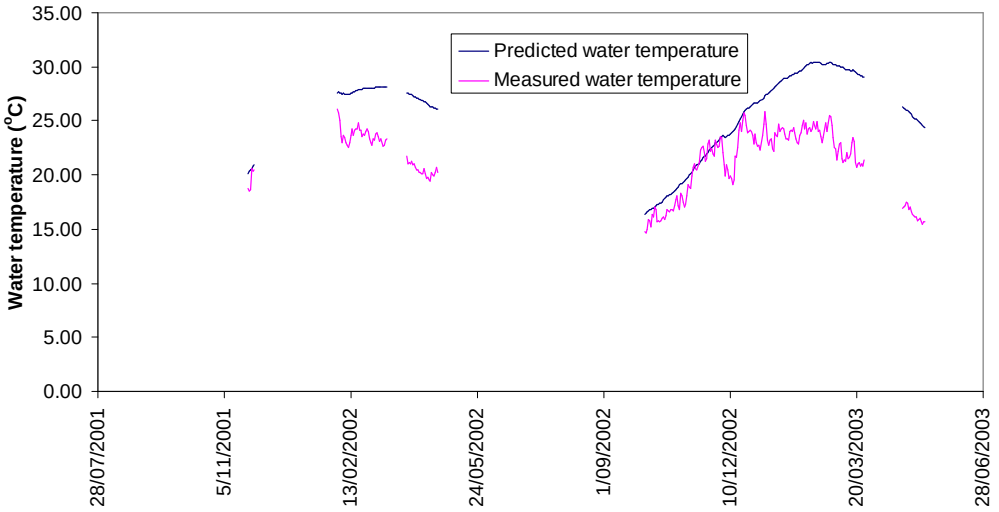

Figure 5-9. Measured and predicted water temperature at Hume Dam

As a result of the overestimation of water temperature, the long-wave radiative energy loss from the system is higher than it would be if the water column were cooler due to the relationship between thermal long-wave emission and temperature. Consequently, the predicted net radiative input is smaller than measured (Figure 5-10).

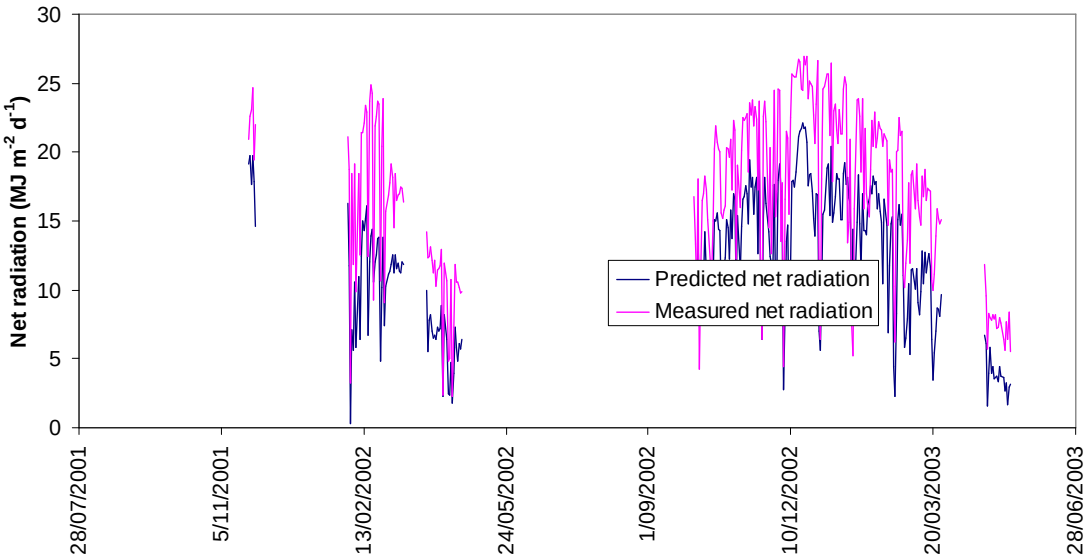

Figure 5-10. Measured and predicted net radiation at Hume Dam

Comparison of interpolated wind speed data for this subcatchment (10 m height) against wind speed measured at the site (2 m height) is shown in Figure 5-11. Clearly the interpolation is grossly under estimating wind speed at

this site. Such differences could well be related to local topographic effects (e.g. valleys – see Figure 5-6) controlling wind speeds, and fetch. Such conditions are very hard to account for in wind speed interpolations from sparse measurement points. Substitution of interpolated wind speed for measured wind speed greatly improves water temperature predictions. However they are still over estimated due to the inability to account for the cooling effect of snow melt inflows.

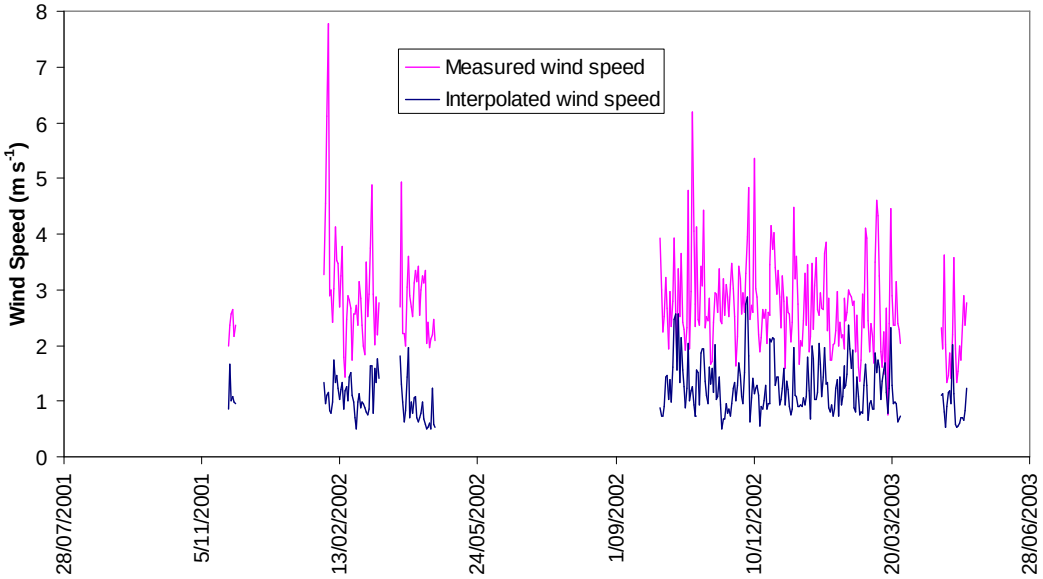

Figure 5-11. Measured (2 m height) and interpolated wind speed (10 m height) at Hume Dam

Because of the poor prediction of water temperatures, wind speed and net radiation, daily evaporation estimates for this complex terrain do not compare well to measurements (Figure 5-12). Despite this, predicted evaporation is only slightly higher than that measured, with total predicted evaporation of 1075 mm compared to the measured 1065 mm. When the estimated wind speed is increased by a factor of two to better match the observed wind speed, the predicted water temperature is within 2 to 3 ℃ of the measured value and the predicted dai ly evaporation is within 0.5 mm d^{-1} of the measured value. A difference of 0.5 mm d^{-1} is equivalent to 100 ML d^{-1} when the reservoir is full.

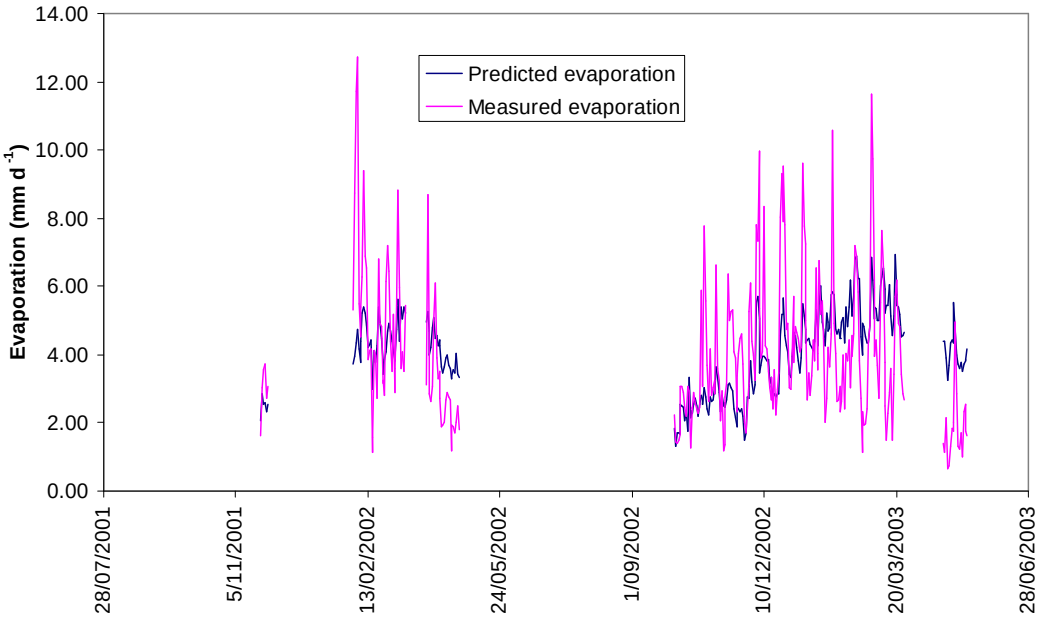

Figure 5-12. Measured and modelled evaporation at Hume Dam

The comparison of the evaporation model with measurements at Hume Dam is summarised in Table 5-4, which includes average daily and monthly measured and modelled water temperature, net radiation and evaporation. Also shown are the standard error of estimates (SEE) and regression coefficient (r^2) for comparison pairs. Difficulties in estimating evaporation at this site are reflected in poor performance in predicting water temperatures and net radiation. While average daily evaporation results compare well, the poor correlation between datasets (r^2 = 0.24) should be noted. The bottom row of the table shows a comparison of scaled pan evaporation (pan coefficient = 0.7) with measured evaporation. This table shows that while scaled pan evaporation is only about 2% below that measured, the correlation between datasets is extremely poor (r^2 = 0.06).

Table 5-4. Daily and monthly measured and modelled results for Hume Dam. Also included for reference are measured and modelled scaled pan evaporation

	Average daily measured	Average daily modelled	% Difference	SEE daily	r^2 daily	SEE monthly	r^2 monthly
Water temperature (℃)	21.4	25.7	20%	2.44	0.52	3.13	0.41
Net radiation (MJ m^{-2} d^{-1})	17.2	12.0	-30%	2.31	0.80	1.05	0.96
Evaporation (mm)	4.0	4.0	1%	1.05	0.24	0.99	0.15
Scaled pan evaporation (mm)	4.0	4.1	2%	1.21	0.06	1.12	0.50

SEE – Standard Error of Estimation.

5.3 Chaffey Dam

5.3.1 Site characteristics

Chaffey Dam is located in northeastern New South Wales in hilly terrain on the Peel River 32 km south-east from Tamworth. The dam is at an altitude of 518 m ASL and has a capacity of 61 GL. Table 5-5 lists the characteristics of the Chaffey Dam site and the measurements available for model testing. Figure 5-13 shows a satellite image of Chaffey Dam from Google Earth 2007. Chaffey Dam falls within the Namoi region of the MDB.

Table 5-5. Site characteristics for Chaffey Dam

Water body location	31°20'56.66"S, 151° 8'13.85"E
Water body area	5.42 km^2
Average water body depth	30 m
Measurement period	September 1995 and October 1997
Measurements	Solar radiation Long-wave radiation Humidity Wind speed Net radiation Water temperature Air temperature Evaporation
Evaporation estimation technique	Stability corrected bulk formula (Liu et al., 1979)
Reference	Sherman et al. (2000a; 2000b)

Figure 5-13. Satellite image of Chaffey Dam

5.3.2 Results

Evaporation at Chaffey Dam was computed using stability-corrected bulk formulae (Liu et al., 1979) developed by Sherman et al. (2000a; 2000b) as part of a project for the CRC for Freshwater Ecology. The dataset includes measurements of long-wave radiation, water temperature, net radiation and evaporation which can be used to test the model. The comparison of the modelled and measured downwelling long-wave radiation inputs (see Figure 5-14) shows very close agreement. Average measured daily downwelling long-wave radiation was 28.6 MJ m^{-2} d^{-1} while the modelled value was 28.9 MJ m^{-2} d^{-1}.

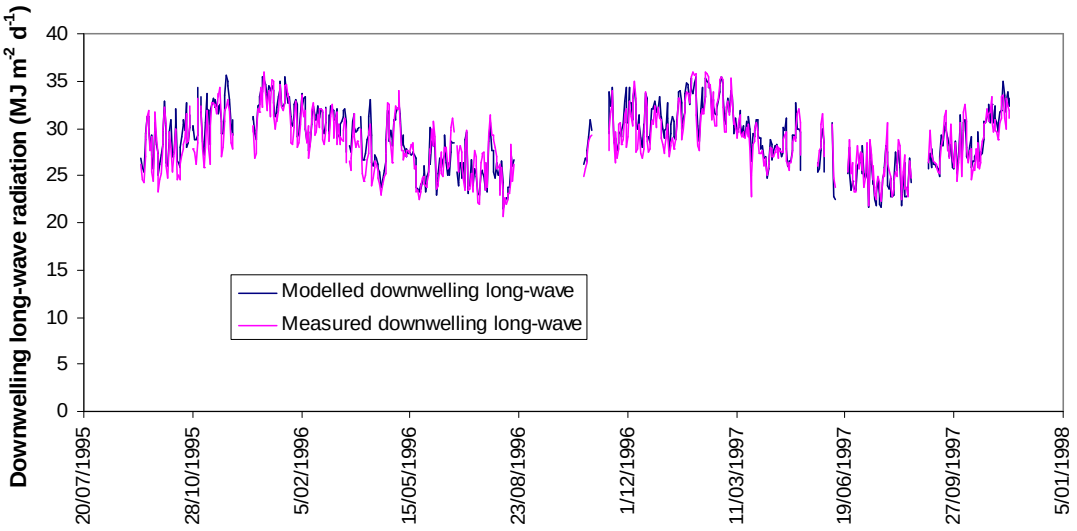

Figure 5-14. Measured and modelled downwelling long-wave radiation at Chaffey Dam

Figure 5-15 shows a comparison of measured and predicted water surface temperature for Chaffey Dam. The model predictions capture the major variations in measured temperature although they were slightly higher than those measured during summer months and slightly lower than those measured during winter months. Average modelled temperature (20.8℃) was slightly higher t han average measured temperature (19.5℃).

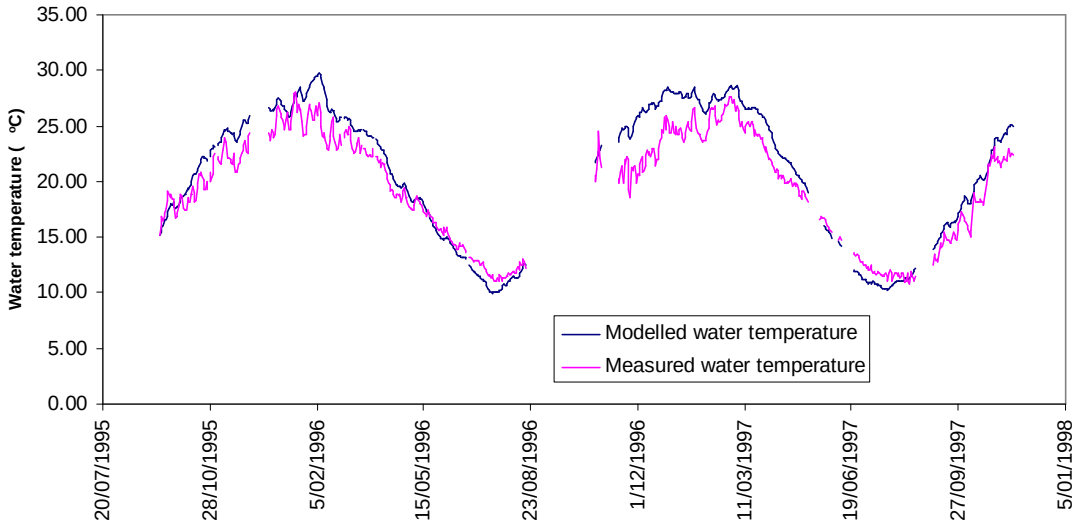

Figure 5-15. Measured and modelled water temperature at Chaffey Dam

Figure 5-16 shows predicted and measured net radiation at Chaffey Dam. Net radiation predictions show similar seasonal differences as measured and modelled water temperature. Average net radiation from the model was 9.6 Wm^{-2} while averaged measured net radiation was 10.6 Wm^{-2}.

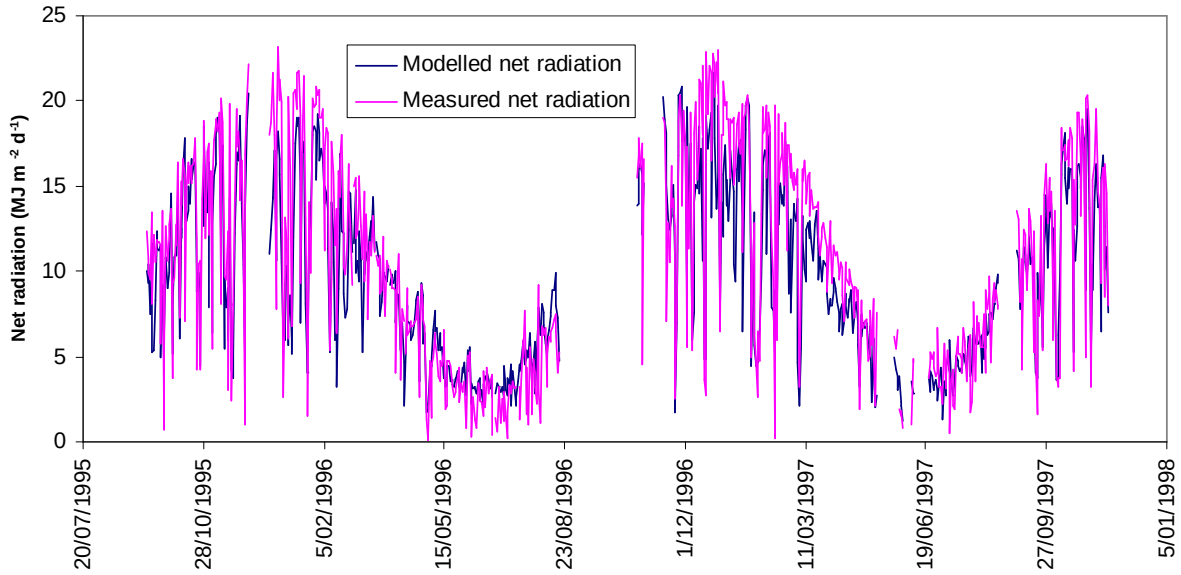

Figure 5-16. Measured and modelled net radiation at Chaffey Dam

Evaporation estimates from measured and modelled datasets are shown in Figure 5-17. The two datasets follow very similar trends throughout the seasons although the measured evaporation rate shows greater variation, possibly as a result of local topographic effects and/or stratification of the water body. Total evaporation from the measurements was 2313 mm with an average rate of 3.6 mm d^{-1}, figures very similar to those from the modelled results where total evaporation was 2422 mm and average daily evaporation rate was 3.7 mm d^{-1}. The total difference over 650 days was just 4%.

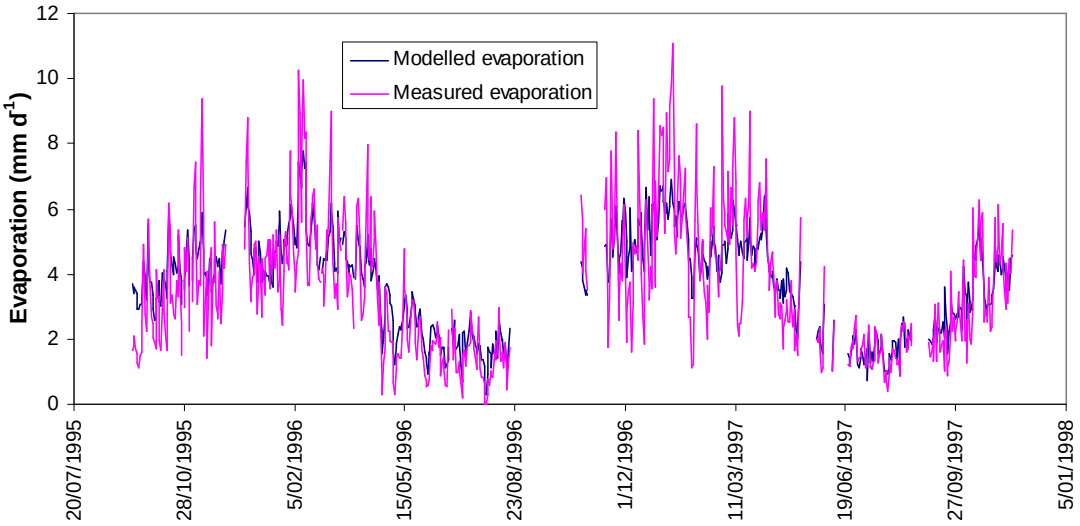

Figure 5-17. Measured and modelled evaporation at Chaffey Dam

The comparison of the evaporation model with measurements at Chaffey Dam is summarised in Table 5-6, which includes average daily and monthly measured and modelled water temperature, net radiation and evaporation. Also shown are the standard error of estimates (SEE) and regression coefficient (r^2) for comparison pairs. Comparison of modelled and measured average daily water temperature, net radiation and evaporation show differences of 6%, -9% and 4%, respectively. The bottom row of the table shows a comparison of scaled pan evaporation (pan coefficient = 0.7) with measured evaporation. This table shows that scaled pan evaporation is much less than that measured and that correlation between the datasets is poor (r^2 = 0.36).

Table 5-6. Daily and monthly measured and modelled results for Chaffey Dam. Also included for reference are measured and modelled scaled pan evaporation

	Average daily measured	Average daily modelled	% Difference	SEE daily	r^2 daily	SEE monthly	r^2 monthly
Water temperature (℃)	19.5	20.8	6%	1.19	0.96	0.97	0.97
Net radiation (MJ m^{-2} d-1)	10.6	9.6	-9%	2.09	0.82	0.96	0.95
Evaporation (mm)	3.6	3.7	4%	0.75	0.75	0.34	0.94
Scaled pan evaporation (mm)	3.6	2.6	-27%	1.09	0.36	0.52	0.77

SEE – Standard Error of Estimation

5.4 Lake Alexandrina and Lake Albert

5.4.1 Site characteristics

Lake Alexandrina and Lake Albert are a pair of lakes adjacent to the coast of the Southern Ocean, about 100 km south-east of Adelaide. These lakes, known as the Lower Lakes, are located in the Murray region of the MDB. Table 5-7 shows the characteristics of both of the lakes and the types of evaporation measurements available for model testing. Figure 5-18 shows a satellite image of Lake Alexandrina and Lake Albert from Google Earth 2007. Four separate studies are available for Lake Alexandrina and Lake Albert; therefore these studies will be dealt with in chronological order.

Table 5-7. Site characteristics for Lake Alexandrina and Lake Albert

Water body location	35°25'47.31"S, 139° 11'25.24"E (Alexandrina) 35°37'6.36"S , 139°17'22.06"E (Albert)
Water body area	570 km^2 (Alexandrina) 180 km^2 (Albert)
Average water body depth	3 m (Alexandrina) 2 m (Albert)
Measurement period	Various between 1971 and 1993 (see text)
Evaporation estimation techniques	Water balance Eddy correlation Energy budget Aerodynamic Bulk transfer
References	Shepherd, 1971; Raupach, 1976; Cheng, 1978; Kotwicki, 1993

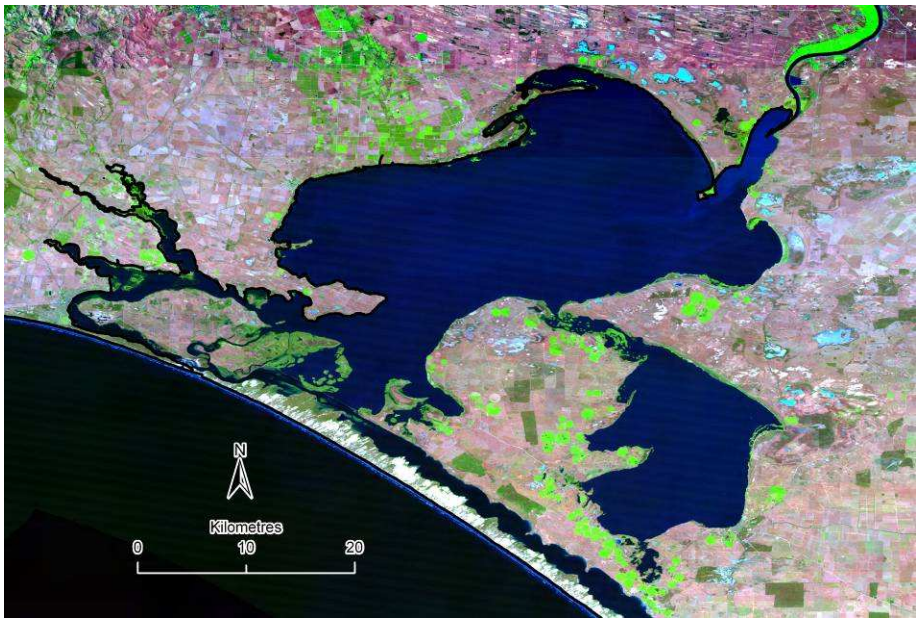

Figure 5-18. Satellite image of Lake Alexandrina (larger water body) and Lake Albert (smaller water body)

5.4.2 Results – Shepherd (1971)

Shepherd (1971) estimated evaporation from lakes Alexandrina and Albert using a water balance method – that is, from measurements of the inflows, outflows, precipitation and changes in water levels. A comparison of monthly evaporation for the lakes for the period from February 1967 to May 1968 is shown in Figure 5-19. Measured and modelled results compare well for the warmer months; however, during the May to July period water balance evaporation rates drop off significantly and in some months actually are calculated to be negative. We hypothesise that what is being observed here is an artefact of the water balance methodology. This methodology calculates evaporation by difference of all other water balance terms, and therefore this estimate has the combined errors of the other components. When evaporation is small and rainfall is high (i.e. winter months) the reliability of estimates is diminished, particularly considering the spatial variability in rainfall for such large lakes and limited number of measurement points used for precipitation estimates. Figure 5-20 shows a comparison of evaporation with pan evaporation for each month. The dataset has been split into two groups based on how they plot with pan evaporation. The split of the data into groups of low and high evaporation rates suggests that there is a systemic difference between the thermodynamics or method of calculating evaporation rate associated with each. Assuming that the dataset for high evaporation rates is the more reliable then we can

compare modelled evaporation with measured evaporation for just those months. This comparison results in total evaporation of 1323 mm for the model and 1280 mm for the water balance results, a difference of just 3% with an r^2 of 0.7. Scaled pan evaporation estimates (pan coefficient = 0.7) for this period results in total evaporation of 1142 mm (11% less than that measured) with a correlation coefficient between measured and estimated evaporation of 0.80. Being a relatively shallow lake system, heat storage is not a large factor controlling seasonal evaporation and, hence, a good correlation between pan and measured evaporation is to be expected.

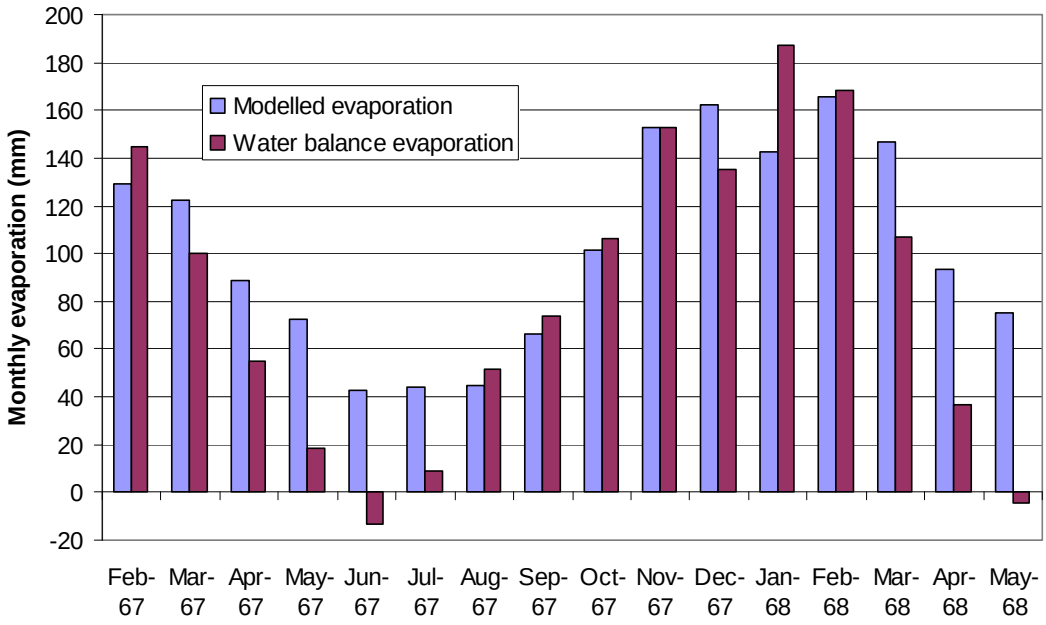

Figure 5-19. Measured and modelled evaporation for Lake Alexandrina and Lake Albert

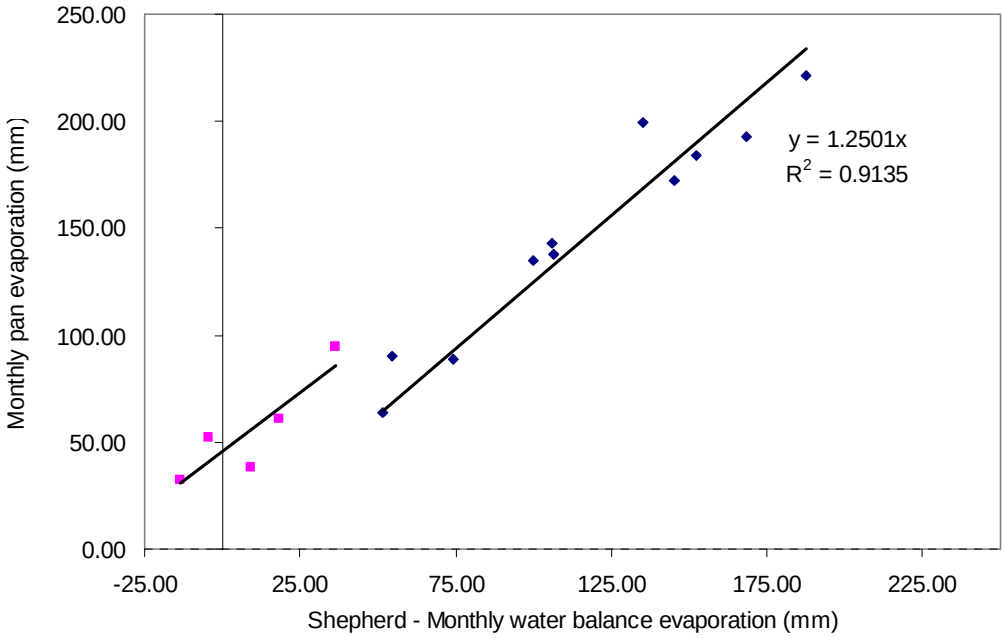

Figure 5-20. Measured and modelled evaporation for Lake Alexandrina and Lake Albert

5.4.3 Results – Raupach (1976)

Raupach (1976) undertook a five-day study of evaporation at Lake Albert during April 1975 using eddy correlation techniques. A comparison of the results of this study with those from our model for the same period are shown in Figure 5-21. It can be seen from this figure that the modelled estimates tend to be lower than those measured using eddy correlation. Average evaporation was 3.21 mm d^{-1} for eddy correlation while the model averaged 2.64 mm d^{-1}. Interestingly, average heat budget and bulk transfer evaporation estimates for these same days (see Kotwicki, 1993) are 2.82 and 3.34 mm d^{-1}, respectively. Our modelled results are not inconsistent within the range of the other estimates especially considering that the measurements were made near the shore whereas ours represent a whole-of-lake estimate.

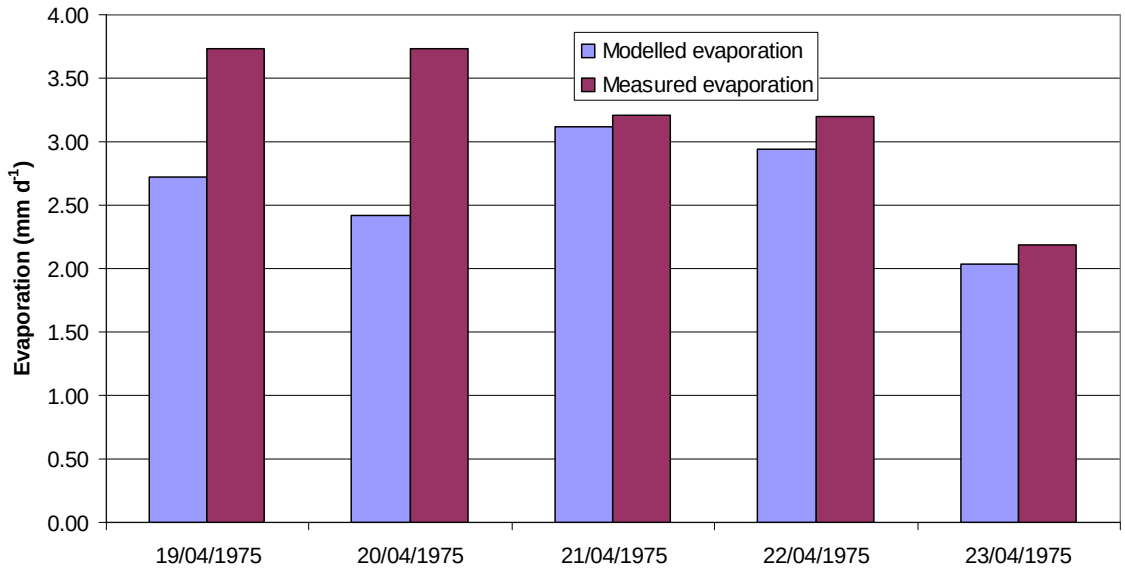

Figure 5-21. Eddy correlation and modelled evaporation at Lake Albert

5.4.4 Results – Cheng (1978)

Cheng (1978) utilised energy budget and aerodynamic methodologies to estimate monthly evaporation for Lake Albert and these results, along with our modelled results for the same period, are shown in Figure 5-22. The three methods track each other nicely across the seasons. For this 12-month period total modelled evaporation was 1330 mm compared to 1286 mm for the energy budget method and 1274 mm for the aerodynamic method. For comparison purposes a further estimate of evaporation for this period was made by using pan evaporation and a scaling factor of 0.7. This resulted in a total evaporation for this period of 1061 mm (~18% less than other estimates) although it should be noted that correlation with other techniques was good (r^2 = 0.8 to 0.9) because of the shallow nature of the lake system which minimises heat storage effects.

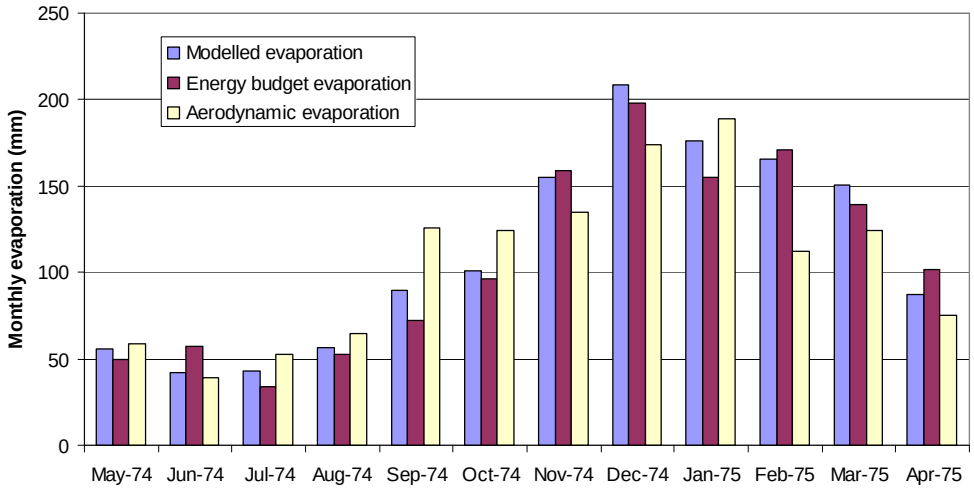

Figure 5-22. Modelled, energy budget and aerodynamic estimates of evaporation at Lake Albert

5.4.5 Results – Kotwicki (1993)

Kotwicki (1993) undertook a study of evaporation from Lake Alexandrina between 1990 to 1992 using bulk transfer techniques. The results of his study are presented in Figure 5-23 along with estimates of evaporation from our modelling technique. Modelled evaporation far exceeds that estimated by Kotwicki, and in fact total evaporation for this period was 3891 mm for the model and 2746 mm for the bulk transfer method. This shows that the model estimates 40% more evaporation (1145 mm) than the bulk transfer method used by Kotwicki. This difference is much larger than found in comparisons between our modelled evaporation rates and those reported by other investigators. Evaporation estimated using pan evaporation and a 0.7 multiplier was 22% less than that modelled.

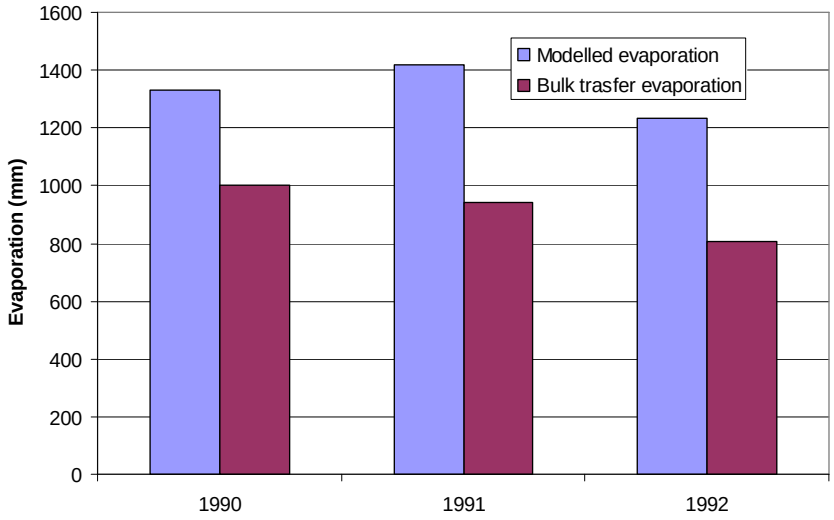

Figure 5-23. Modelled and bulk transfer estimates of evaporation at Lake Alexandrina

5.5 Maude Weir

5.5.1 Site characteristics

Maude Weir is located on the Murrumbidgee River, 53 km west of Hay in New South Wales. It is at an altitude of 76 m ASL. Maude Weir raises the water level of the Murrumbidgee River to a pool depth of between 6.0 and 6.3 m for diversions into the Lowbidgee irrigation areas and also holds back the winter flow of the Murrumbidgee thereby permitting flushes of water during the summer months. Although the weir is only 6 m deep the river backs up behind the weir for 30 km because of the small river slope. This weir is typical of many of this sort in the MDB. Table 5-8 shows the characteristics of the Maude Weir and the measurements available for model testing.

Table 5-8. Site characteristics for Maude Weir

Water body location	34°28'40.95"S, 144°18'7.81"E
Water body width	60 m
Average water body depth	6 m
Measurement period	December 1993 to April 1995
Measurements	Solar radiation Long-wave radiation Humidity Wind speed Water temperature Evaporation
Evaporation estimation technique	Heat budget
Reference	Sherman et al., 1998; Webster et al., 1996

5.5.2 Results

The dataset of Sherman et al. (1998) and Webster et al. (1996) includes measurements of long-wave radiation, water temperature and evaporation which can all be used to test the model. Figure 5-24 shows good agreement between observed and predicted downwelling long-wave radiation. Average for the model was 32.4 MJ m^{-2} d^{-1} while the measured average downwelling long-wave radiation was 30.9 MJ m^{-2} d^{-1}.

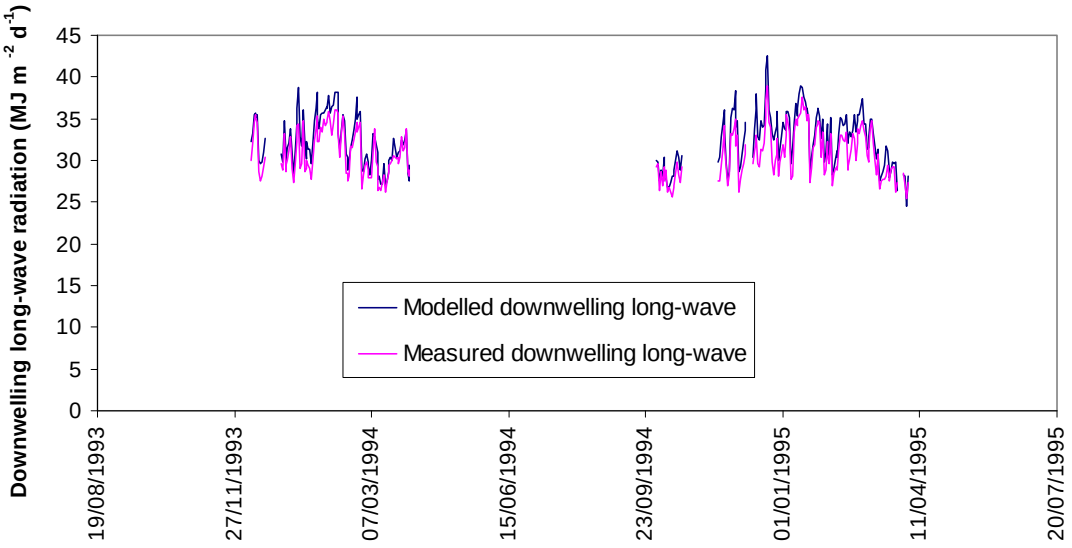

Figure 5-24. Measured and modelled downwelling long-wave radiation at Maude Weir

Measured and modelled water temperatures also closely matched although the modelled values did not respond as quickly as those measured (Figure 5-25). Average modelled water temperature was 25.1 ℃ while measu red was 24.4 ℃. As a result of the good representation of water temperature in the model, modelled upwelling long-wave radiation was also very similar to that measured (Figure 5-26). Average modelled upwelling long-wave radiation was 37.7 MJ m^{-2} d^{-1} while measured was 37.3 MJ m^{-2} d^{-1}.

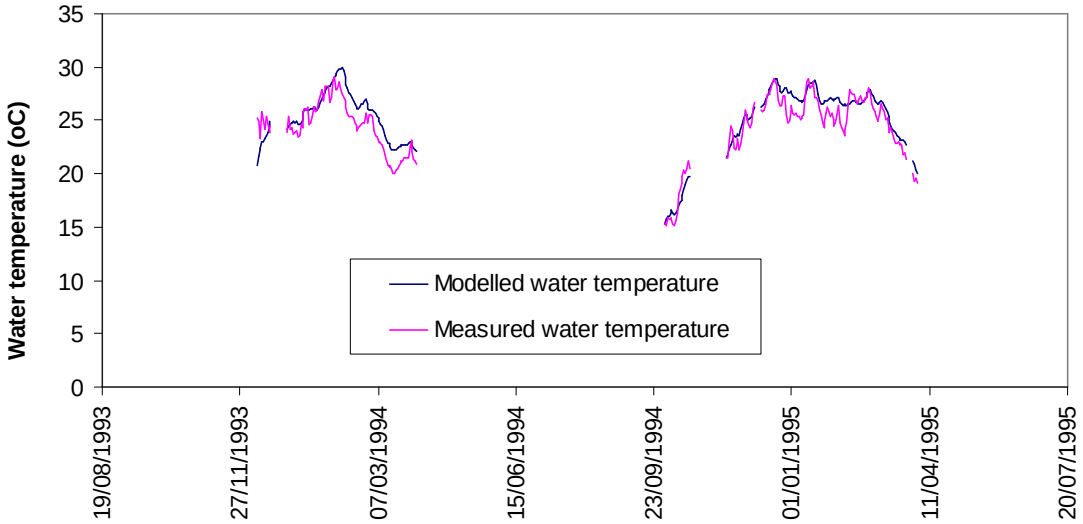

Figure 5-25. Measured and modelled water temperature at Maude Weir

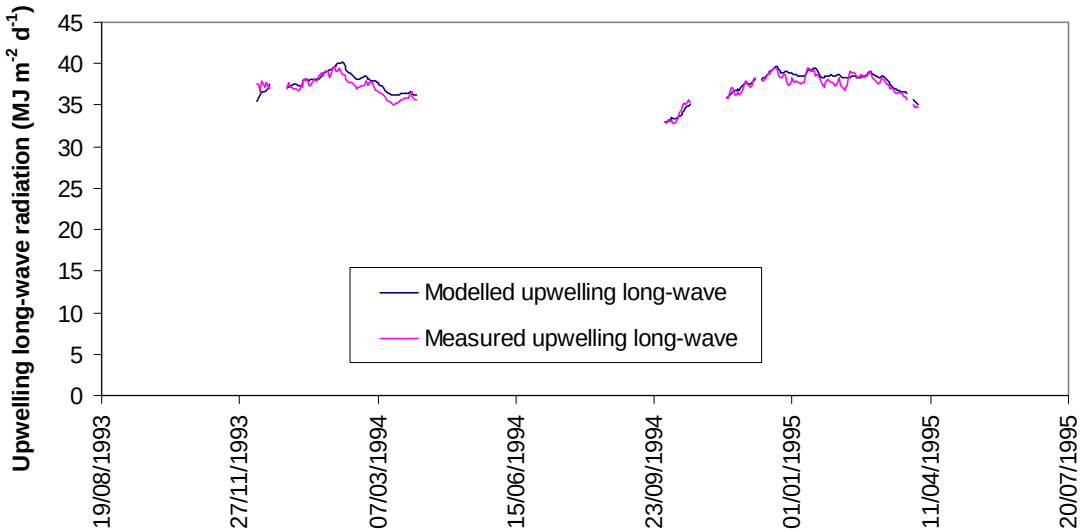

Figure 5-26. Measured and modelled upwelling long-wave radiation at Maude Weir

With good approximations of long-wave radiation, modelled and measured net radiation also compared well (Figure 5-27). Average for the modelled dataset was 16.8 MJ m^{-2} d^{-1} while measured was 15.7 MJ m^{-2} d^{-1}.

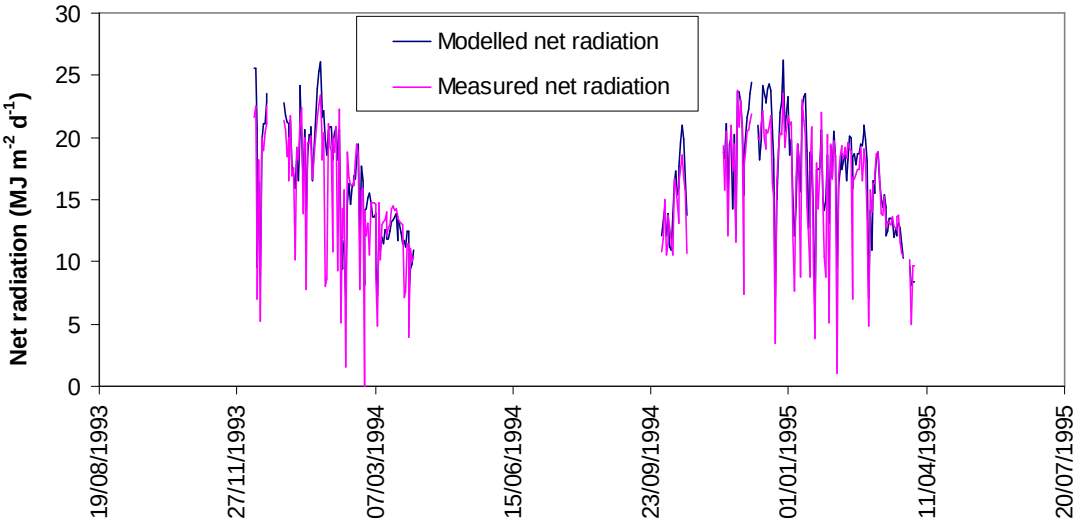

Figure 5-27. Measured and modelled net radiation at Maude Weir

Comparison of modelled and measured evaporation rates for Maude Weir pool are shown in Figure 5-28. Modelled evaporation is compared to two measurement estimates: those using an aerodynamic approach and those using a heat budget approach. Over the entire period, average evaporation rates are quite different and the timing of peaks and troughs in the records often do not align. The modelled average daily evaporation was 6.7 mm, the aerodynamic average daily was 4.1 mm and the heat budget average daily was 5.8 mm. It is interesting to note that the heat budget estimate was less than the modelled estimate during the first section of data (January to March 1994) but was often much higher in the later section (January to April 1995). The aerodynamic estimate was consistently low. Comparison of wind speed used in the modelled and measured techniques (Figure 5-29) show that wind speed is generally slightly higher from the interpolated dataset than from the local measurements over water. This difference is not enough to explain the differences in evaporation rate. However, the different peak and troughs suggest that wind direction may be an important factor at this site. The weir pool was bordered by a band of trees. Wind blowing through the trees would be subject to higher levels of turbulence than winds blowing along the channel so the relationship between wind speed and evaporation rate is certain to be affected by wind direction.

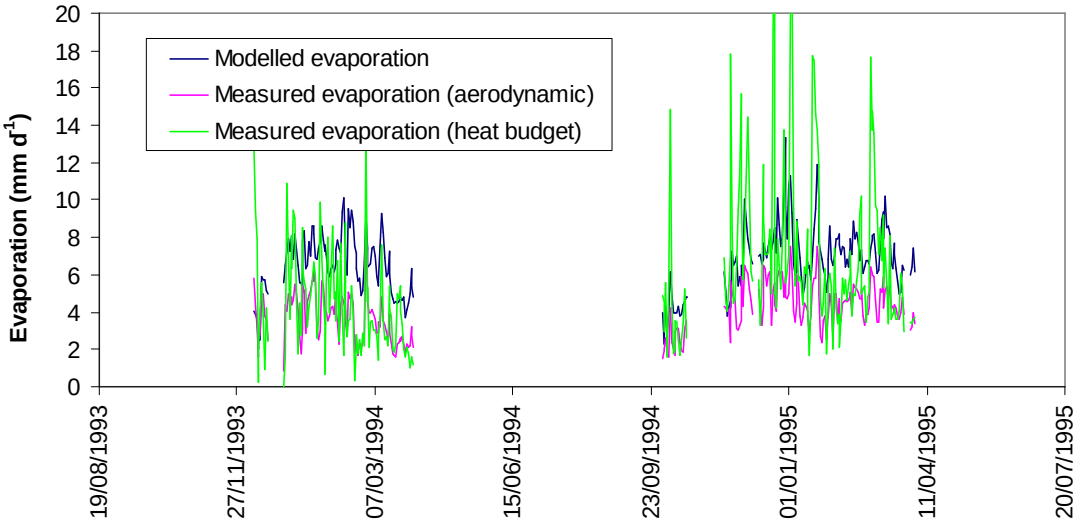

Figure 5-28. Measured and modelled evaporation at Maude Weir (Measured evaporation includes aerodynamic and heat budget approaches.)

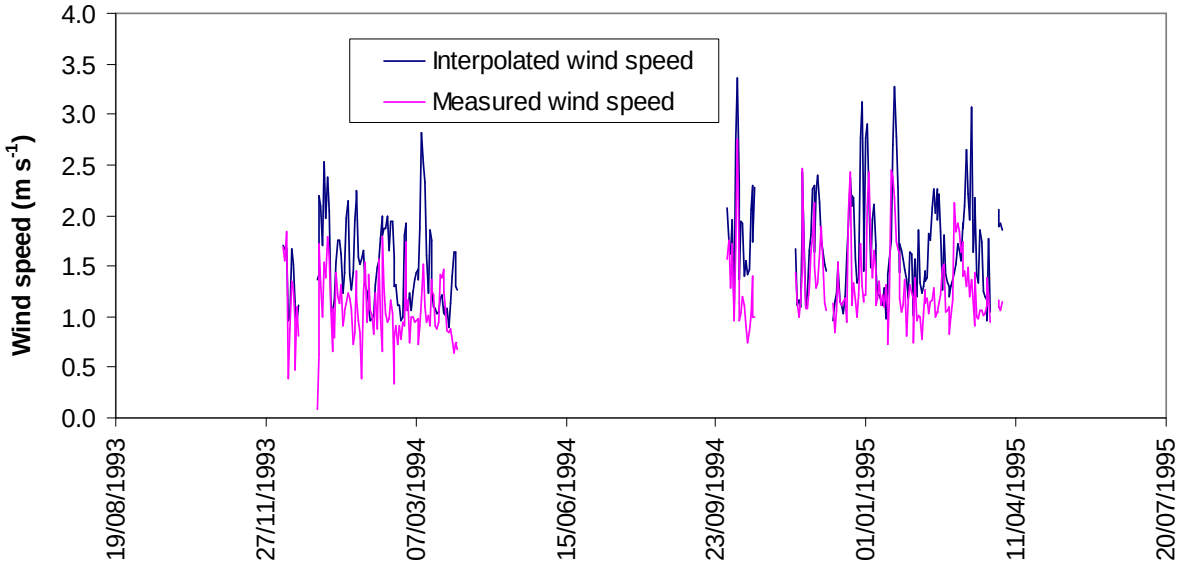

Figure 5-29. Interpolated and measured wind speed at Maude Weir

To explore the issue of wind direction further, wind speed over water was compared with that measured in a nearby paddock. Wind roses were constructed for the two periods of data covering January to March 1994 (Figure 5-30) and January to February 1995 (Figure 5-31). The channel of Maude Weir pool is aligned roughly on the west–east axis. During the first period of comparison it is clear that the wind speed over land (right plot in Figure 5-30) is from the SSE; however, winds from this direction do not feature prominently on the measurements above water where winds seem to be predominantly from a westerly direction. It is believed that this effect is due to the sheltering effect of vegetation along the banks which restricts winds from the north and south whereas winds from the west or east blow directly along the channel. This observation explains the overestimation of evaporation by the model during this early period of comparison. During the second period (January to February 1995) predominant winds over the land (right plot in Figure 5-31) are more from westerly and easterly directions (i.e. along the channel) and as a result this is when evaporation estimates are most similar. Comparing results for the second period only shows evaporation estimates of 4.34, 6.91 and 6.89 mm d^{-1} for aerodynamic, modelled and heat budget methods, respectively. Obviously the presence of riparian vegetation and channel orientation influences evaporation rates; however it is not possible to account for all of the factors over a basin the size of the MDB.

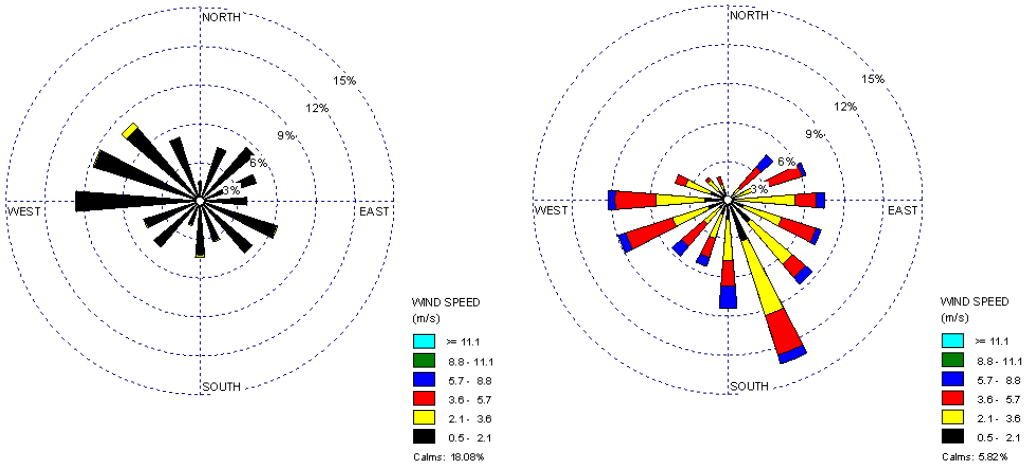

Figure 5-30. Wind roses for wind speed measured over water (left) and over land (right) for January to March 1994

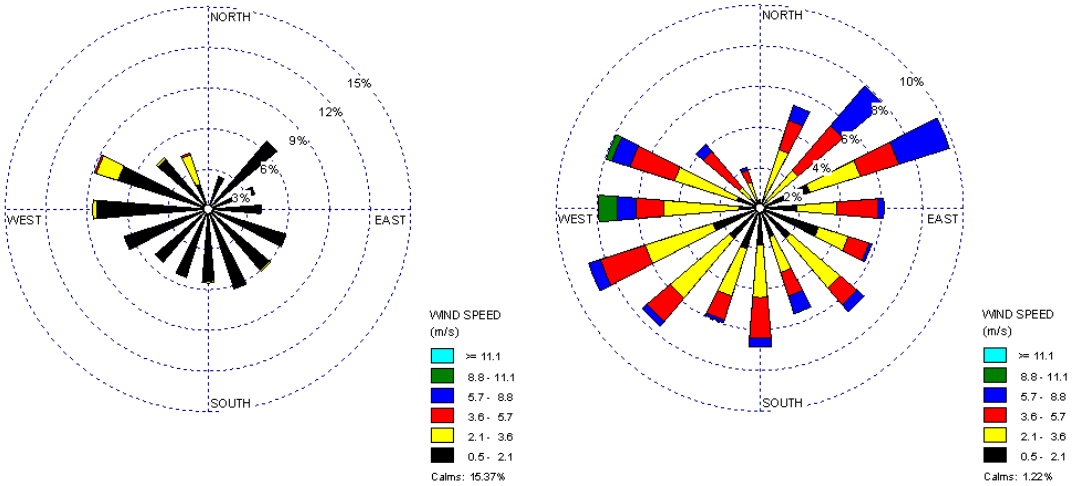

Figure 5-31. Wind roses for wind speed measured over water (left) and over land (right) for January to February 1995

The comparison of the evaporation model with measurements at Maude Weir is summarised in

Table 5-9, which includes average daily and monthly measured and modelled water temperature, net radiation and evaporation via different methods. Difficulties in estimating evaporation at this site due to local wind fields is demonstrated by the low r^2 values between measured and modelled estimates. The bottom row of the table shows a comparison of scaled pan evaporation (pan coefficient = 0.7) with measured evaporation (aerodynamic method). This table shows that scaled pan evaporation is only about 6% above that measured but that correlation between the two datasets is not so good (r^2 = 0.19).

Table 5-9. Daily and monthly measured and modelled results for Maude Weir. Also included for reference are measured and modelled scaled pan evaporation estimates

	Average daily measured	Average daily modelled	% Difference	SEE daily	r^2 daily	SEE monthly	r^2 monthly
Water temperature (℃)	24.0	25.5	6%	1.38	0.87	0.90	0.92
Net radiation (MJ m^{-2} d^{-1})	13.9	14.3	3%	1.46	0.72	0.56	0.98
Evaporation: aerodynamic method (mm)	5.3	5.9	11%	0.32	0.30	0.98	0.52
Evaporation: heat budget method (mm)	5.8	5.9	1%	1.59	0.15	1.15	0.34
Scaled pan evaporation (mm)	5.3	5.6	7%	1.59	0.19	0.65	0.68

SEE – Standard Error of Estimation

5.6 Tatura Irrigation Channel

5.6.1 Site characteristics

A study of evaporation from irrigation channels was undertaken by McLeod (1993) near the town of Tatura in northern Victoria. Tatura is at an altitude of about 100 m ASL. Table 5-10 shows the characteristics of the irrigation channel and the measurements available for model testing. The Tatura irrigation study falls within the Goulbourn-Broken region of the MDB.

Table 5-10. Site characteristics for irrigation channel near Tatura

Water body location	Somewhere in the vicinity of Tatura
Water body width	4.5 m (assumed)
Average water body depth	2 m (assumed)
Measurement period	1990 and 1991
Measurements	Evaporation Pan evaporation
Evaporation estimation technique	Heat budget
Reference	McLeod (1993)

5.6.2 Results

In his work on the evaporation from irrigation channels near Tatura using the heat budget method, McLeod (1993) does not report evaporation rates for clearly defined days. He does, however, present figures showing relationships between daily heat budget evaporation and pan evaporation from the nearby Institute of Sustainable Irrigated Agriculture (ISIA) in Tatura. The dates of McLeod's study may not be specified but we know they occurred during 1990 and 1991. For comparison purposes, we ran our model for the entire 1990 to 1991 period and plotted results against pan evaporation from ISIA (Figure 5-32).

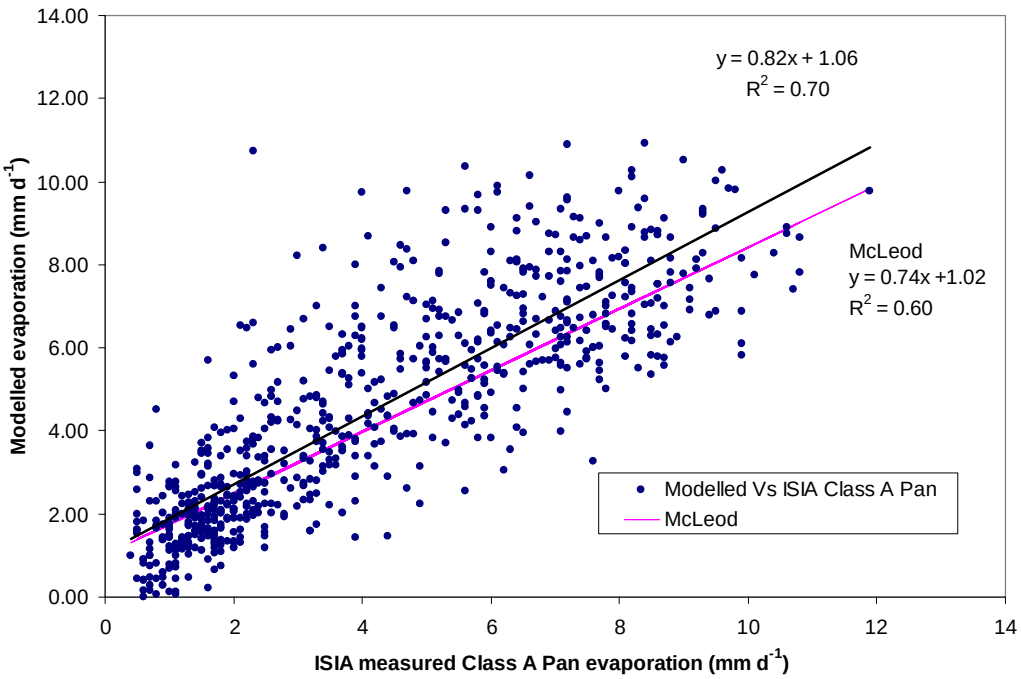

Figure 5-32. Modelled evaporation plotted against Class A Pan evaporation from ISIA. The regression line in pink is the relationship reported by McLeod (1993)

The relationship between modelled and pan evaporation is not particularly strong but this was also the case for the relationships reported by McLeod (1993). The slope and intercept of the modelled dataset and the regression reported by McLeod are very similar (Figure 5-32) giving confidence in the modelled results for irrigation channels. Application of the equation from both datasets to the ISIA Class A Pan evaporation data results in an annual average evaporation of 1626 mm for our model and 1491 mm for the relationship derived by McLeod – a difference of 9%.

While no measured time series data is available for this site, the comparison of measured with modelled evaporation rates for this location suggests that the model is making reasonable evaporation estimates. Therefore we can use these estimates to test the performance of evaporation estimates based on evaporation pan data and a pan coefficient of 0.7 (Figure 5-33). This figure shows that the two estimates show the same seasonal trends although scaled pan evaporation is consistently below evaporation model estimates (40% less over the whole time series). A regression analysis of these two datasets shows a strong linear relationship ($r^2 = 0.76$) illustrating that a site-specific pan factor would produce reasonable estimates at this location. This comparison serves to illustrate that pan factors may be applicable to seasonal/monthly estimations of evaporation from small shallow water bodies but that they are likely to be site specific, hence reducing the attractiveness of using such techniques for estimates in the Murray-Darling Basin Sustainable Yields Project.

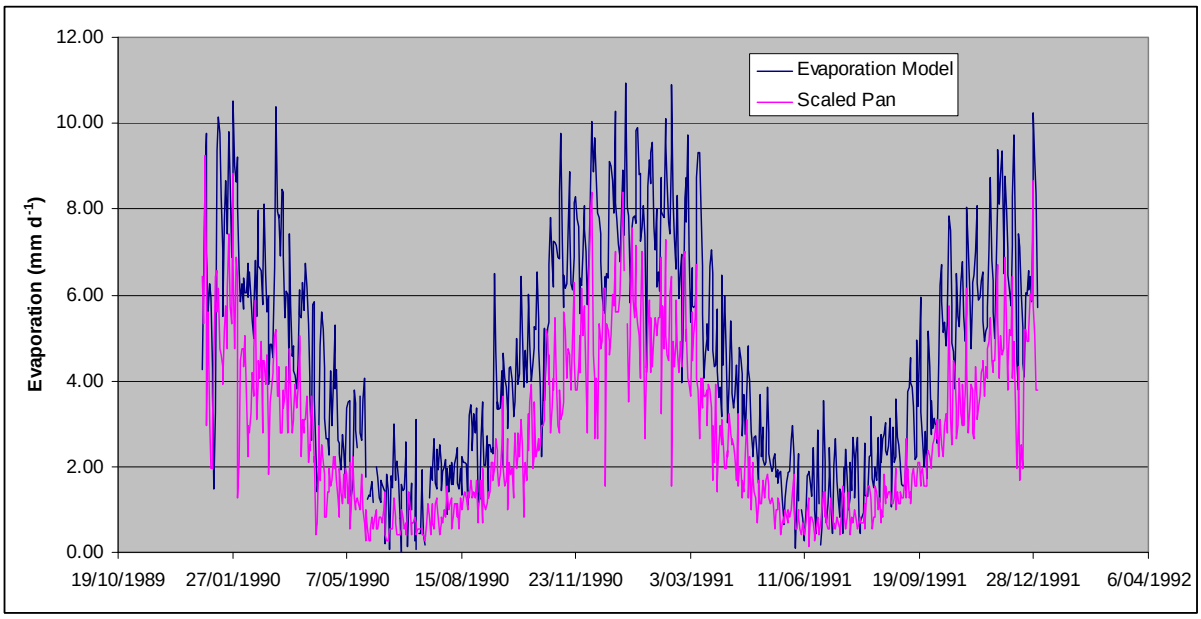

Figure 5-33. Modelled and scaled pan evaporation estimates of evaporation for an irrigation channel in Tatura

5.7 Summary

Comparison of modelled and measured evaporation from seven test sites shows generally good model performance across a range of water body types and sizes. On average, differences between observed and modelled estimates of daily evaporation were less than 10%. Radiation inputs, both long-wave and short-wave, are represented well by the model resulting in differences between observed and modelled net radiation of less than 5% (excluding Hume Reservoir where observed and interpolated wind speeds were very different and snow melt inputs were likely). Water temperatures – which are a measure of the accuracy of the combined heat fluxes including the latent heat of evaporation – are impressively predicted in all locations (less than 6% difference in daily averages) except in Hume Reservoir where the error in interpolated wind data caused the estimated water temperature to be much higher than measured resulting in overestimation of evaporation rate. The presence of riparian vegetation and channel orientation influences evaporation rates from narrow meandering water bodies. However, accounting for such factors for all individual water bodies is well beyond the scope of a study for a basin the size of the MDB. Wind interpolation from scattered measurements does not take into account topographic influences at smaller scale which will also potentially contribute to errors in the local estimation of wind speed used by the evaporation model. Comparison of the evaporation model with evaporation estimates using evaporation pan coefficients shows that the key advantages of the evaporation model are that it can account for water body depth and size, which in turn allows accurate estimates of seasonal evaporation variations to be made. In summary, this analysis suggests that the evaporation model can provide reliable estimates of evaporation from different sizes of water bodies across the MDB, but that this accuracy can be compromised by local factors such as surrounding vegetation and topography.

6 Model uncertainty

The model input variables most likely to produce uncertainty in estimates of evaporation include: (i) air temperature, (ii) solar radiation, (iii) vapour pressure, (iv) wind speed, (v) water body depth, and (vi) water body size. The aim of this section is to assess the consequences of data error on the accuracy of the computation of evaporation rates assuming that the model is a sufficiently accurate representation of reality. The following analysis of uncertainty is based in subcatchment number 4120261 (Lachlan @ Oxley). This subcatchment was selected because of its central location in the MDB. For the analysis a 17-year time series (1990 to 2006) of SILO and wind speed data was used. As is the case for application of the model to the whole MDB, average subcatchment SILO data (average of all 0.5° grid points in subcatchment) and wind data (average of all pixel values in subcatchment) were used. The standard deviations of these input parameters were also calculated from the source datasets. Average subcatchment altitude and latitude and their standard deviations were used. The water body used in the analysis was set to 1 km^2 in area and 4 m deep. In addition to the six input variables listed above, altitude and latitude are also input variables that can potentially affect model evaporation estimates. Altitude influences the transmissivity of the atmosphere and hence clear sky solar radiation estimates, while latitude affects sun angles and extraterrestrial solar radiation estimates. The analysis shows that the uncertainty associated with using these two variables is much less than 1% so they will not be considered in the analysis below. Information regarding the seasonal bias in SILO estimates is currently not available but if such errors are large (i.e. summer radiation consistently over estimated) the influence on evaporation amount and timing is likely to be large.

6.1 Air temperature

An analysis of the accuracy of interpolation of SILO data was undertaken by Jeffrey et al. (2001). It was shown that predictions of maximum and minimum temperature in the MDB were predicted very well. Mean absolute error for minimum temperature in the MDB was less than 1.5 ℃ while mean absolute error in maximum temperature was less than 1.3 ℃. Our model uses mean daily temperature and therefore the uncertainty analysis will assume a uncertainty of ±1.5 ℃. We have also calculated the standard deviation (SD) of the datasets used to make the subcatchment average dataset so we will also analyse our data with an uncertainty of ±SD.

Figure 6-1 shows the impact of a ±1.5 ℃ temperature variation on evaporation estimates for the test water body. The mean absolute error in interpolated temperature reported by Jeffrey et al. (2001) results in evaporation uncertainty of ±5%. The evaporation estimates based on the ±SD of the averaged datasets resulted in variation in evaporation of ±3%.

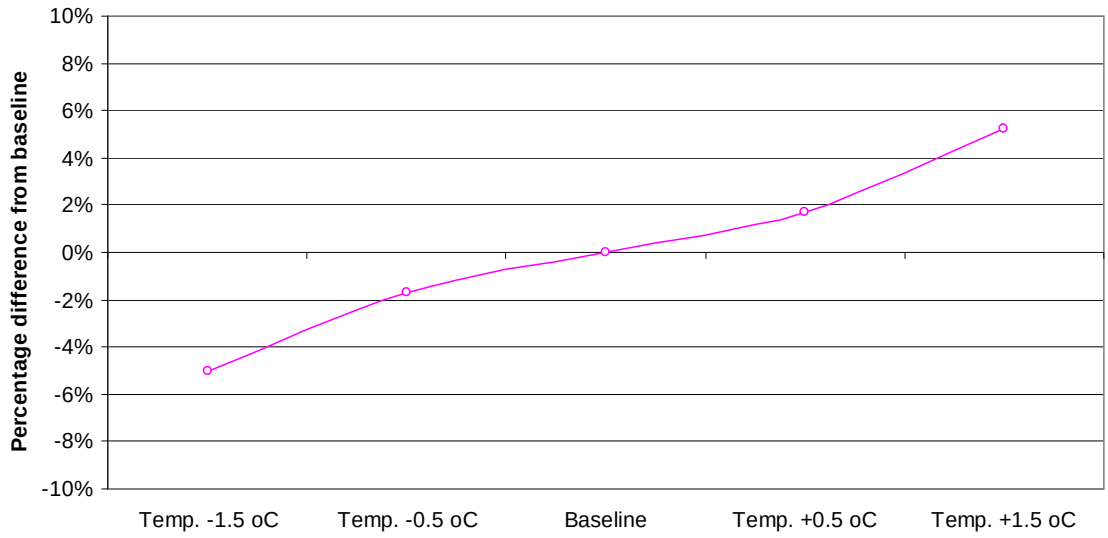

Figure 6-1. Effect of temperature uncertainty on evaporation estimates

6.2 Solar radiation

Jeffrey et al. (2001) did not analyse the accuracy of interpolation of solar radiation in SILO data. Therefore, a different methodology was needed to set uncertainty bounds. Using the test datasets from Maude Weir, Hume Dam and Chaffey Dam we compared measured solar radiation with that from the subcatchment average SILO data. Differences in total solar radiation for the respective measurements period were 1% for Maude Weir, 3% for Hume Dam and 4% for Chaffey Dam. In the following analysis we will use a range of solar radiation estimates of ±5%. The subcatchment average standard deviation has also been calculated and used in a similar analysis.

Figure 6-2 shows the impact of a ±10% solar radiation variation on evaporation estimates for the test water body. This analysis shows an evaporation uncertainty of ±6%. The evaporation estimates based on the ±SD of the averaged datasets resulted in variation in evaporation of ±3%.

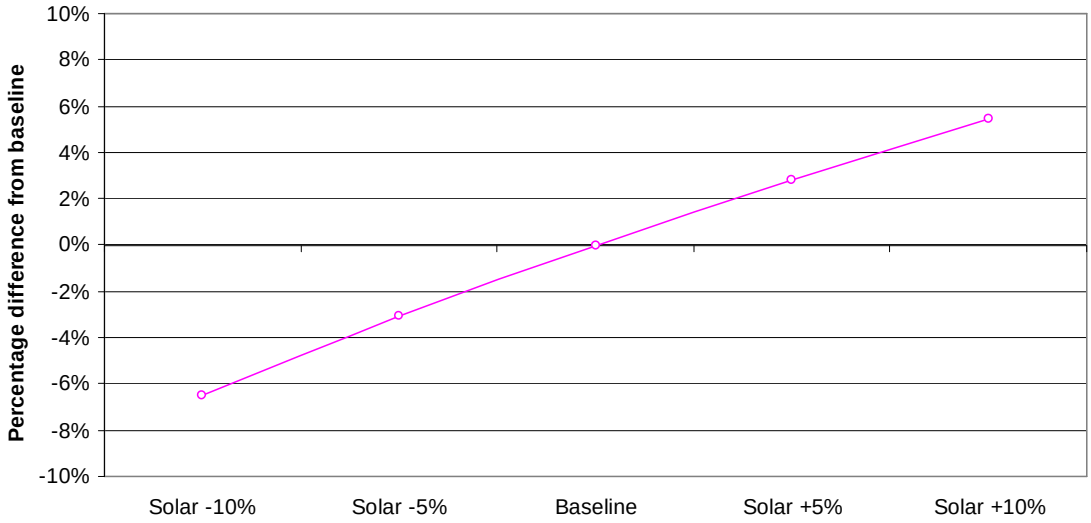

Figure 6-2. Effect of solar radiation uncertainty on evaporation estimates

6.3 Vapour pressure

Jeffrey et al. (2001) calculated the mean absolute error for vapour pressure interpolations from the SILO dataset. They showed that predictions of vapour pressure in the MDB were very good. Mean absolute error for vapour pressure in the MDB was less than 1.5 hPa (0.15 kPa). Using these results we will assume an uncertainty of ±0.15 kPa in our analysis. We have also analysed for the standard deviation of the subcatchment average dataset. Figure 6-3 shows the impact of a ±0.15 kPa vapour pressure variation on evaporation estimates for the test water body. The mean absolute error in interpolated vapour pressure reported by Jeffrey et al. (2001) results in evaporation uncertainty of less than ±3%. The evaporation estimates based on the ±SD of the averaged datasets resulted in variation in evaporation of ±1%.

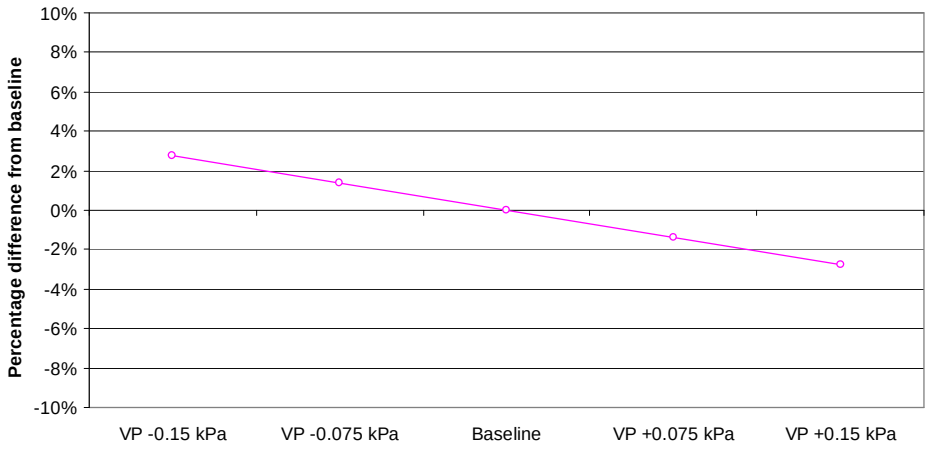

Figure 6-3. Effect of vapour pressure uncertainty on evaporation estimates

6.4 Wind speed

At this stage the wind speed dataset used in this project does not include measurement uncertainty. With the knowledge that wind speed is highly variable with topography and altitude we have assumed an uncertainty of ±50%. We have also analysed for the standard deviation of the subcatchment average dataset.

The results of this analysis are shown in Figure 6-4. Underestimation of wind speed by 50% results in underestimation of evaporation by 7% while over estimation of wind speed by 50% results in overestimation by 5%. The evaporation estimates based on the ±SD of the subcatchment averaged datasets resulted in variation in evaporation of <±1% meaning there was little variation in wind speed across this catchment.

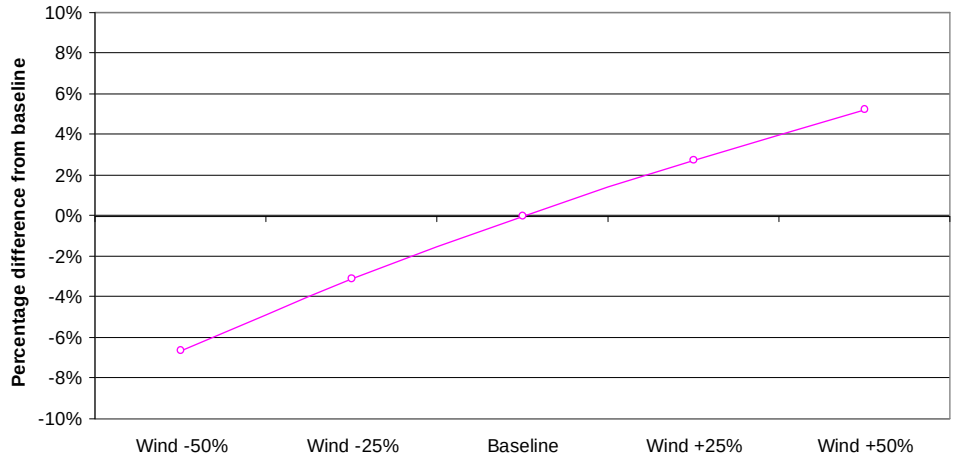

Figure 6-4. Effect of wind speed uncertainty on evaporation estimates

6.5 Water body depth

The evaporation model uses set depths for different water bodies for evaporation rate estimates (see Table 4-3). The depth of the test water body is 4 m and to test the effect of depth on evaporation estimates an uncertainty of ±2 m will be used. Figure 6-5 shows that uncertainty in depth has very little effect of evaporation estimates with ±2 m resulting in much less than ±1% change in evaporation. The effect of depth is more related to the temporal pattern of evaporation than the absolute total. Increasing depth results in increased heat storage during warming months and release through the cooling months. Therefore increasing the depth tends to cause a decrease in evaporation rate during the time of the year when the water column is warming during spring and early summer and an increase in rate when the water column is cooling.

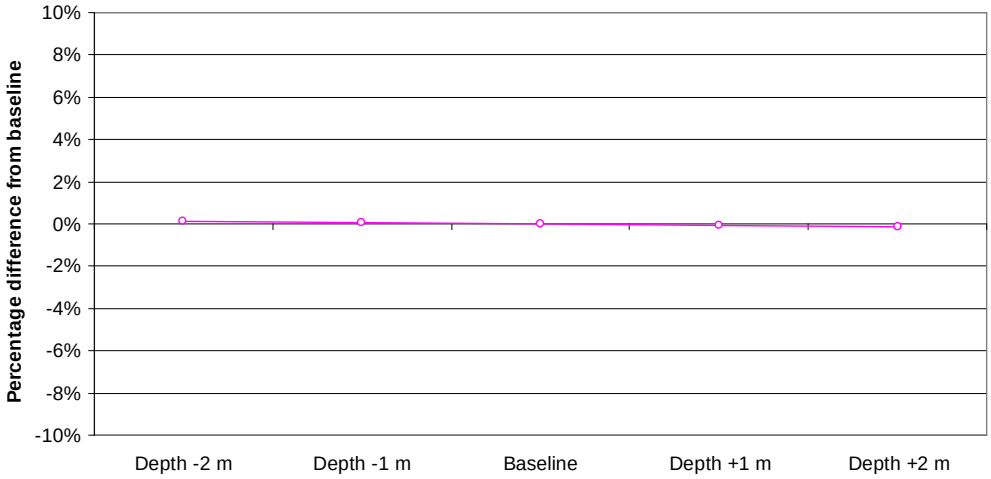

Figure 6-5. Effect of water body depth uncertainty on evaporation estimates

6.6 Water body area

The effect of water body area on evaporation estimates is twofold. First, the rate of water loss as volume per time is equal to the product of the evaporation rate (rate of volume loss per area) and surface area. Thus, an error in

area of 10% will cause an error in evaporation loss rate of 10% (Figure 6-6). Also, in our methodology larger water bodies have a smaller evaporation rate than smaller ones (Equation 6) although the proportional change in rate is much less than the proportional rate in area (<1%). This justifies using a small number of characteristic water body types and sizes to represent evaporation from a continuum of water body dimensions (Table 4-3).

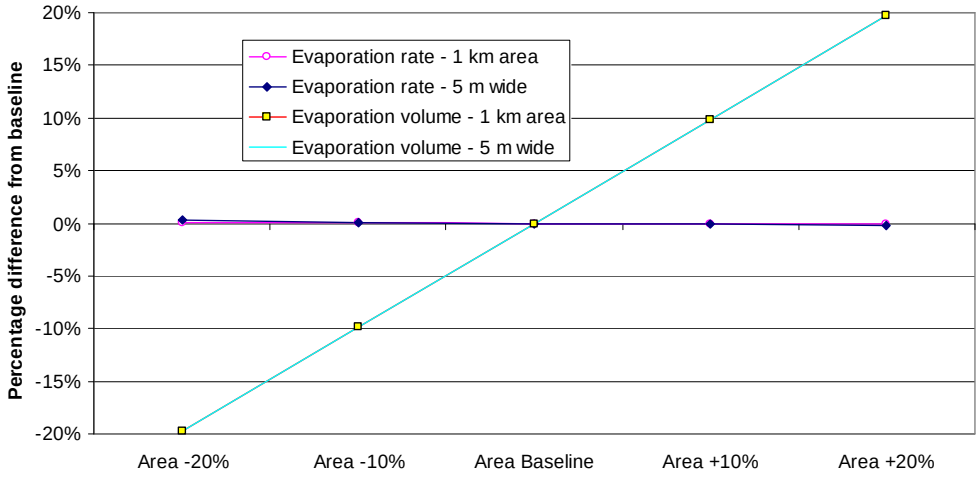

Figure 6-6. Effect of water area uncertainty on evaporation estimates

6.7 Summary

This analysis of uncertainty has revealed that the modelled evaporation rates are insensitive to uncertainty and variation in altitude, latitude and area (Table 6-1). On a seasonally averaged basis, water body depth has little effect on water loss, but will modify the intensity and timing of the seasonal evaporation cycle. The model is also sensitive to errors in wind speed although we believe that by assuming such a large uncertainty (±50 %) we are capturing the likely error from this source in our model. The model was sensitive to uncertainty in solar radiation input, but comparisons between SILO estimated radiation and measured radiation suggest that the SILO radiation is an accurate representation of reality so that the error to predicted evaporation rates is judged to be small for the intended application. The primary source of error in evaporation volume estimates is the water surface area, as total evaporation scales directly with surface area. This is particularly important to the MDB where much of the input data regarding water body area is static in time. For example, this does not allow for variation in reservoir area with time due to inflows, drawdown, evaporation or irrigation channels not always being active. Such information for a catchment as large as this does not yet exist. It is also worth noting that this uncertainty analysis does not include analysis of the influence of seasonal bias in SILO estimates on evaporation timing and amount. Seasonal bias could produce more uncertainty than underestimation and overestimation of parameters over time.

Table 6-1. Summary of uncertainty analysis for input variables

Input data	Input uncertainty	Evaporation uncertainty
Temperature	±1.5 ℃	±3%
Solar radiation	±10%	±6%
Vapour pressure	±0.15 kPa	±3%
Wind speed	±50%	±7%
Altitude	±50%	±1%
Latitude	±2°	±1%
Water depth	±2 m	±1%
Water area (evaporation rate)	±20%	±1%
Water area (evaporation volume)	±20%	±20%

7 Conclusions

A review of the literature and available techniques for estimating evaporation identified ‘combination methods’ as the most appropriate for estimating evaporation from open water in the MDB based on the available datasets. The combination method used was the Penman-Monteith method with an adjustment to the amount of energy available for evaporation based on changes in heat storage within the water body. Such adjustments are made by estimating the temperature of the water using equilibrium temperature concepts. Details of all algorithms used for each step in the calculations have been presented.

Testing of the model against measured datasets from seven different locations showed that the model was able to produce reliable estimates of the radiation budget, water temperature and evaporation of water bodies from irrigation channels to large reservoirs. Model predictions of evaporation rates are about 10% greater than corresponding estimates using the heat budget and aerodynamic methods. The methodology for estimating evaporation assumes a flat landscape around the water body and there is some indication that the method is less accurate for systems where fringing trees or riparian vegetation are present.

Analysis of the uncertainty of estimated evaporation due to the uncertainty in input variables showed that the model was sensitive to errors in solar radiation and wind speed. However, this uncertainty was believed to be at the limit of what would be expected from input datasets. Utilisation of subcatchment average values did not have significant effects on the uncertainty of model estimates. Correct specification of water area was identified as the primary source of error in evaporation volume estimates. This is important to note because very little is known about the dynamic nature of water bodies in the MDB; clearly improved data in this area would reduce the uncertainty in model estimates.

In summary the open water evaporation model developed for the MDB is suitable for assessing evaporation from different water bodies of a range of sizes over such a large area. The model runs on readily available datasets and produces reliable results.

8 References

Allen RG, Pereira LS, Raes D, Smith M (1998) Crop evapotranspiration - Guidelines for computing crop water requirements. FAO - Food and Agriculture Organization of the United Nations: Rome; pp 300.

Anderson ER (1954) Energy budget studies. Water-loss investigations: Lake Hefner studies. U.S. Geological Survey. Professional Paper 269; 71-119.

Calder IR, Neal C (1984) Evaporation from saline lakes: a combination equation approach. Hydrological Sciences Journal **29**: 89-97.

Cheng W (1978) A study of evaporation from Lake Albert, using meteorological and hydrological observations In School of Earth Sciences. Flinders University; pp. 193.

Dalton J (1802) Experimental essays on the constitution of mixed gases; on the force of steam or vapour from water and other liquids at different temperatures, both in a Torricellian vacuum and in air; on evaporation; and on the expansion of gases by heat. Memoirs of the Literary and Philosophical Society of Manchester 5-11: 535-602.

de Bruin HAR (1982) Temperature and energy balance of a water reservoir determined from standard weather data of a land station. Journal of Hydrology 59: 261-274.

Edinger JE, Duttweiler DW, Geyer JC (1968) The response of water temperature to meteorological conditions. Water Resources Research 4: 1137-1143.

Finch JW, Hall RL (2001) Estimation of open water evaporation. A review of methods. Environment Agency, Bristol; 155.

Gangopaghaya M, Harbeck GE, Nordenson TJ, Omar MH, Uryvaev VA. 1966. Measurement and Estimation of Evaporation and Evapotranspiration. World Meteorological Organization: Geneva; 121 pp.

Hounam CE (1973) Comparison between pan and lake evaporation. World Meteorological Organisation.

Idso SB, Jackson RD (1969) Thermal radiation from the atmosphere. Journal of Geophysical Research 74: 5397-5403.

Jeffrey SJ, Carter JO, Moodie KB, Beswick AR (2001) Using spatial interpolation to construct a comprehensive archive of Australian climate data. Environmental Modelling and Software with Environment Data News 16: 309-330.

Jegede OO, Ogolo EO, Aregbesola TO (2006) Estimating net radiation using routine meteorological data at a tropical location in Nigeria. International Journal of Sustainable Energy 25: 107-115.

Jensen ME, Burman RD, Allen RG (1990) Evapotranspiration and irrigation water requirements. American Society of Civil Engineers: New York.

Keijman JQ, Koopmans RWR (1973) A comparison of several methods of estimating evaporation of Lake Flevo In Hydrology of lakes. IAHS publication no 109: Helsinki; 225-232.

Khan S, Rana T, Beddek R, Blackwell J, Paydar Z, Carroll J (2004) Whole of catchment water and salt balance to identify potential water saving options in the Murrumbidgee catchment. CSIRO Land and Water; 86.

Kirby M, Van Dijk AIJM, Mainuddin M, Peña-Arancibia J, Guerschman J-P, Liu Y, Marvanek S, McJannet DL, Paydar Z, McVicar TR, Van Niel TG, Li LT (2008) River Water Balance Accounts Across the MDB, 1990-2005. A report to the Australian Government from the CSIRO Murray-Darling Basin Sustainable Yields Project. CSIRO, Australia.

Kotwicki V (1993) Evaporation from Lake Alexandrina. The Flinders University of South Australia, PhD thesis.

Lapworth CF (1965) Evaporation from a reservoir near London. Journal of the Institution of Water and Environmental Management 19: 163-181.

Leopold LB, Maddock T (1953) The hydraulic geometry of stream channels and some physiographic implications. USGS Professional Paper 252.

Leopold LB, Wolman MG, Miller JP (1964) Fluvial Processes in Geomorphology. Freeman and Company, San Francisco, California; 522.

Liu WT, Katsaros KB, Businger JA (1979) Bulk parameterization of the air-sea exchange of heat and water vapor including the molecular constraints at the interface. Journal of Atmospheric Science 36: 1722-1735.

McLeod AJ (1993) Measurement and modelling of irrigation channel seepage in northern Victoria In Department of Civil Engineering. University of Melbourne.

McMillan W (1973) Cooling from open water surfaces: Final Report, Part 1: Lake Trawsfynydd cooling investigation. Scientific Services Department, CEGB Manchester.

McVicar TR, Van Niel TG, Li LT, Roderick ML, Donohue RJ, Rayner DP. (In prep.) Spatially distributing near-surface wind speed climatology and trends of Australia. Geophysical Research Letters.

Monteith JL (1965) Evaporation and the environment. In The state and movement of water in living organisms*,* Fogg GE (ed). Cambridge University Press: London.

Oke TR (1987) Boundary Layer Climates. Methuen & Co.: London; 435.

Penman HL (1948) Natural evaporation from open water, bare soil and grass. Proceedings of the Royal Society of London Series A 193: 120-145.

Rahman JM, Seaton SP, Perraud J-M, Hotham H, Verrelli DI, Coleman JR (2003) It's TIME for a new environmental modelling framework In Modelling and Simulation Society of Australia and New Zealand, Townsville*,* Post DA ed.; 1727-1732.

Raupach MR (1976) Atmospheric flux measurements by eddy correlation. The Flinders University of South Australia.

Shepherd KJ (1971) Evaporation losses from Lake Alexandrina and Albert during the 1967-8 drought. South Australian Government. The Engineering and Water Supply Department; 15.

Sherman BS (2005) Hume Reservoir thermal monitoring and modelling - final. Report for State Water as agent for the Murray-Darling Basin Commission. CSIRO Land and Water Client Report. Canberra: CSIRO Land and Water. CSIRO Land and Water; pp. 100.

Sherman BS, Ford P, Hatton T, Whittington J, Green D, Baldwin DS, Oliver R, Shiel R, van Berkel J, Beckett R, Grey L, Maher B (2000a) The Chaffey Dam Story. CRC for Freshwater Ecology; pp. 150.

Sherman BS, Webster IT, Jones GJ, Oliver RL (1998) Transitions between Aulacoseira and Anabaena dominance in a turbid river weir pool. Limnology and Oceanography 43: 1902-1915.

Sherman BS, Whittington J, Oliver RL (2000b) The impact of artificial destratification on water quality in Chaffey Reservoir. Arch. Hydrobiol. Spec. Issues Advanc. Limnol. Limnology and Lake Management 2000+ 55: 15–29. Arch. Hydrobiol. Spec. Issues Advanc. Limnol. Limnology and Lake Management 2000+ 55: 15-29.

Stanhill G (1976) The CIMO international evaporimeter comparisons. World Meteorological Organisation, Geneva; 38 pp.

Stewart RB, Rouse WR (1976) A simple method for determining evaporation from shallow lakes and ponds. Water Resources Research 12: 623-628.

Sweers HE (1976) A nomograph to estimate the heat-exchange coefficient at the air-water interface as a function of wind speed and temperature; a critical survey of some literature. Journal of Hydrology 30: 375-401.

Webster I, Jones G, Oliver R, Bormans M, Sherman B (1996) Control strategies for cyanobacterial blooms in weir pools. .

Webster IT, Sherman BS (1995) Evaporation from fetch-limited water bodies Irrigation Science 16: 53-64.

9 Appendix A: List of symbols

Symbol	Description	Units
D	Date of data	dd/mm/yyyy
T_a	Mean daily air temperature	℃
e_a	Daily vapour pressure (taken as 9:00 am)	kPa
$K\downarrow$	Total daily incoming short-wave radiation	MJ m^{-2} d^{-1}
U_{10}	Average daily wind speed at 10 m	m s^{-1}
Z	Water depth (could be a time series if required)	m
ψ	Water body altitude	m
φ	Latitude	radians
A	Water body area	km^2
ρ_w	Density of water (1000 kg m^{-3})	kg m^{-3}
C_w	Specific heat of water (0.004185 MJ kg^{-1} ℃ $^{-1}$)	MJ kg^{-1} ℃ $^{-1}$
ρ_a	Density of air (1.2 kg m^{-3})	kg m^{-3}
C_a	Specific heat of air (0.001013 MJ kg^{-1} ℃ $^{-1}$)	MJ kg^{-1} ℃ $^{-1}$
σ	Stefan-Boltzmann constant (4.9E-09 MJ m^{-2} ℃ $^{-4}$ d^{-1})	MJ m^{-2} ℃ $^{-4}$ d^{-1}
k	von Karmen constant (0.41 m)	m
z	Height of wind speed measurements (10 m)	m
z_o	Roughness length of momentum and water (0.001 m)	m
α	Albedo of water (0.08)	-
λ	Latent heat of vaporisation	MJ kg^{-1}
γ	Psychometric constant	kPa ℃ $^{-1}$
T_d	Dew point temperature	℃
T_n	Wet-bulb temperature	℃
Δ_n	Slope of the temperature saturation water vapour curve at wet bulb temperature	kPa ℃ $^{-1}$
J	Day of the year	-
d_r	Inverse relative distance Earth-Sun	-
δ	Solar decimation	-
X	X-factor	-
ϖ_s	Sunset hour angle	-
K_{ET}	Extraterrestrial short-wave radiation	MJ m^{-2} d^{-1}
K_{Clear}	Clear sky short-wave radiation	MJ m^{-2} d^{-1}
K_{Ratio}	Ratio of incoming short-wave radiation to clear sky short-wave radiation	-
ε	Emissivity for water	-
$L\downarrow$	Incoming long-wave radiation	MJ m^{-2} d^{-1}

Symbol	Description	Units
$L\uparrow_n$	Outgoing long-wave radiation at wet-bulb temperature	MJ m^{-2} d^{-1}
Q^*_n	Net radiation at wet-bulb temperature	MJ m^{-2} d^{-1}
$f(u)$	Wind function	MJ m^{-2} d^{-1} kPa^{-1}
T_e	Equilibrium temperature	℃
τ	Time constant	days
T_w	Water temperature	℃
$L\uparrow$	Outgoing long-wave radiation	MJ m^{-2} d^{-1}
Q^*	Net radiation	MJ m^{-2} d^{-1}
e^*_w	Saturation vapour pressure at water temperature	kPa
Δ_w	Slope of the temperature saturation water vapour curve at water temperature	kPa ℃ $^{-1}$
N	Change in heat storage in the water body	MJ m^{-2} d^{-1}
r_a	Aerodynamic resistance	s m^{-1}
E	Evaporation from the water body	mm d^{-1}
E_{ML}	Volumetric evaporation loss	ML
Q_a	Mean annual flow	ML
Q_{bf}	Flow at bank flow	ML d^{-1}
Q	Flow	ML d^{-1}
L	Channel width	m
L_{bf}	Channel width at bankfull	m
$\overline{W}$	Effective channel width	m

10 Appendix B: Model algorithms

Evaporation (E in mm d^{-1}) from a water body can be estimated using the Penman-Monteith equation (Monteith, 1965):

$$E = \frac{1}{\lambda}\left(\frac{\Delta_w(Q^* - N) + 86400\rho_a C_a(e_w^* - e_a)/r_a}{\Delta_w + \gamma}\right)$$ Equation 7

where ρ_a is density of air (kg m^{-3}) and C_a is specific heat of air (MJ kg^{-1} $^oK^{-1}$).

Latent heat of vaporisation, λ (MJ kg^{-1}), at air temperature, T_a (℃), is calculated as follows:

$$\lambda = 2.501 - T_a 2.361\times10^{-3}$$ Equation 8

The psychometric constant, γ (kPa ℃ $^{-1}$) is calculated from:

$$\gamma = \frac{C_a 100}{0.622\lambda}$$ Equation 9

Aerodynamic resistance, r_a (s m^{-1}), is calculated using the following equation (Calder and Neal, 1984):

$$r_a = \frac{\rho_a C_a}{\gamma(f(u)/86400)}$$ Equation 10

The wind function, $f(u)$ (MJ m^{-2} d^{-1} kPa^{-1}), is calculated from wind speed at 10 m, U_{10} (m s^{-1}), and area, A (km^2), (Sweers, 1976):

$$f(u) = \left(\frac{5}{A}\right)^{0.05}(3.80 + 1.57U_{10})$$ Equation 11

Net radiation, Q^* (MJ m^{-2} d^{-1}), is calculated using solar radiation inputs, $K\downarrow$ (MJ m^{-2} d^{-1}), as follows:

$$Q^* = K\downarrow(1-\alpha) + (L\downarrow - L\uparrow)$$ Equation 12

Incoming long-wave radiation, $L\downarrow$ (MJ m^{-2} d^{-1}), is calculated from the equations of Oke (1987) and Idso and Jackson (1969):

$$L\downarrow = (C_f + (1-C_f)(1-(0.261\exp(-7.77\times10^{-4}T_a^{\,2}))))\sigma(T_a + 273.15)^4$$ Equation 13

Equations 14 though 21 are used to calculate $L\downarrow$. Fraction of cloud cover (value from 0 to 1 with 1 being 100% cover) is calculated using the following equation (Jegede et al., 2006):

If K_{Ratio} ≤ 0.9 then use $C_f = 1.1 - K_{Ratio}$ Equation 14

If K_{Ratio} > 0.9 then use $C_f = 2(1 - K_{Ratio})$

Ratio of incoming short-wave radiation to clear sky short-wave radiation (K_{Ratio}) is calculated from:

$$K_{Ratio} = \frac{K\downarrow}{K_{Clear}}$$ Equation 15

Clear sky short-wave radiation (K_{Clear} in MJ m^{-2} d^{-1}) is calculated using water body altitude (ψ in m) as follows (Allen et al., 1998):

$$K_{Clear} = (0.75 + 2\times10^{-5}\psi)K_{ET}$$ Equation 16

Extraterrestrial short-wave radiation (K_{ET} in MJ m^{-2} d^{-1}) is calculated using latitude (φ in radians) as follows:

$$K_{ET} = \frac{24(60)}{\pi}0.082d_r(\varpi_s \sin(\varphi)\sin(\delta) + \cos(\varphi)\cos(\delta)\sin(\varpi_s))$$ Equation 17

Sunset hour angle, ϖ_s, is calculated from:

$$\varpi_s = \frac{\pi}{2} - \arctan\left(\frac{-\tan(\varphi)\tan(\delta)}{X^{0.5}}\right)$$ Equation 18

The X-factor, X, is calculated from:

$$X = 1 - (\tan(\varphi))^2(\tan(\delta))^2$$ Equation 19

Solar decimation, δ, is calculated using the day of the year, J, as follows:

$$\delta = 0.409\sin\left(\frac{2\pi}{365}J - 1.39\right)$$ Equation 20

The inverse relative distance Earth-Sun, d_r, is calculated using:

$$d_r = 1 + 0.033\cos\left(\frac{2\pi}{365}J\right)$$ Equation 21

Outgoing long-wave radiation at water temperature ($L\uparrow$ in MJ m^{-2} d^{-1}) is calculated using the Stefan-Boltzmann constant, σ (MJ m^{-2} ^{o}K^{-4} d^{-1}), as follows:

$$L\uparrow = 0.97\sigma(T_w + 273.15)^4$$ Equation 22

Equations 23 through 29 are used to calculate $L\uparrow$. Water temperature, T_w (℃), is calculated from the following equation (de Bruin, 1982):

$$T_w = T_e + (T_{w0} - T_e)\exp(-1/\tau)$$ Equation 23

Equilibrium temperature, T_e (℃), is calculated from the following equation (d e Bruin, 1982):

$$T_e = T_n + \frac{Q^*_n}{4\sigma(T_n + 273.15)^3 + f(u)(\Delta_n + \gamma)}$$ Equation 24

Wet-bulb temperature, T_n (℃), is calculated using vapour pressure, e_a (kPa), as follows (Jensen et al., 1990):

$$T_n = \frac{0.00066 \times 100 T_a + (4098 e_a / (T_d + 237.3)^2) T_d}{0.00066 \times 100 + (4098 e_a / (T_d + 237.3)^2)}$$ Equation 25

Dew point temperature, T_d (℃), is calculated from:

$$T_d = \frac{116.9 + 237.3 Ln(e_a)}{16.78 - Ln(e_a)}$$ Equation 26

Slope of the temperature saturation water vapour curve at wet bulb temperature, Δ_n (kPa ℃ $^{-1}$), is calculated from:

$$\Delta_n = \frac{4098\left[0.6108 \exp\left(\frac{17.27 T_n}{(T_n + 237.3)}\right)\right]}{(T_n + 237.3)^2}$$ Equation 27

Net radiation at wet-bulb temperature, Q^*_n (MJ m^{-2} d^{-1}), is calculated using albedo, α, as follows:

$$Q^*_n = K\downarrow(1-\alpha) + (L\downarrow - L\uparrow_n)$$ Equation 28

Outgoing long-wave radiation at wet-bulb temperature, $L\uparrow_n$ (MJ m^{-2} d^{-1}), is calculated from:

$$L\uparrow_n = \sigma(T_a + 273.15)^4 + 4\sigma(T_a + 273.15)^3 (T_n - T_a)$$ Equation 29

The time constant (τ in days) is calculated using the density of water (ρ_w in kg m^{-3}), specific heat of water (C_w in MJ kg^{-1} ^{o}K^{-1}), and depth of water (Z in m) as follows (de Bruin, 1982):

$$\tau = \frac{\rho_w C_w Z}{4\sigma(T_n + 273.15)^3 + f(u)(\Delta_n + \gamma)}$$ Equation 30

Change in heat storage in the water body, N (MJ m^{-2} d^{-1}), is calculated from:

$$N = \rho_w C_w Z (T_w - T_{w0})$$ Equation 31

Saturated vapour pressure at water temperature, e_w^* (kPa), is calculated from:

$$e_w^* = 0.6108 \times \exp\left(\frac{17.27 T_w}{T_w + 237.3}\right)$$ Equation 32

Slope of the temperature saturation water vapour curve at water temperature, Δ_w (kPa ℃ $^{-1}$), is calculated from:

$$\Delta_w = \frac{4098\left[0.6108 \times \exp\left(\frac{17.27 T_w}{(T_w + 237.3)}\right)\right]}{(T_w + 237.3)^2}$$ Equation 33

11 Appendix C: Model framework

The open water evaporation model was developed using the CRC for Catchment Hydrology's TIME modelling framework (Rahman et al., 2003). The framework is based around the core EquibTemp model which contains the algorithms described in Section 3. In this way the model allows for the structured and automated simulation of a large number of catchments within the MDB, each of which contains a number of subcatchments. Each subcatchment in turn contains a number of water body types such as rivers and lakes which can be modelled with either static or dynamic areas for any given time period.

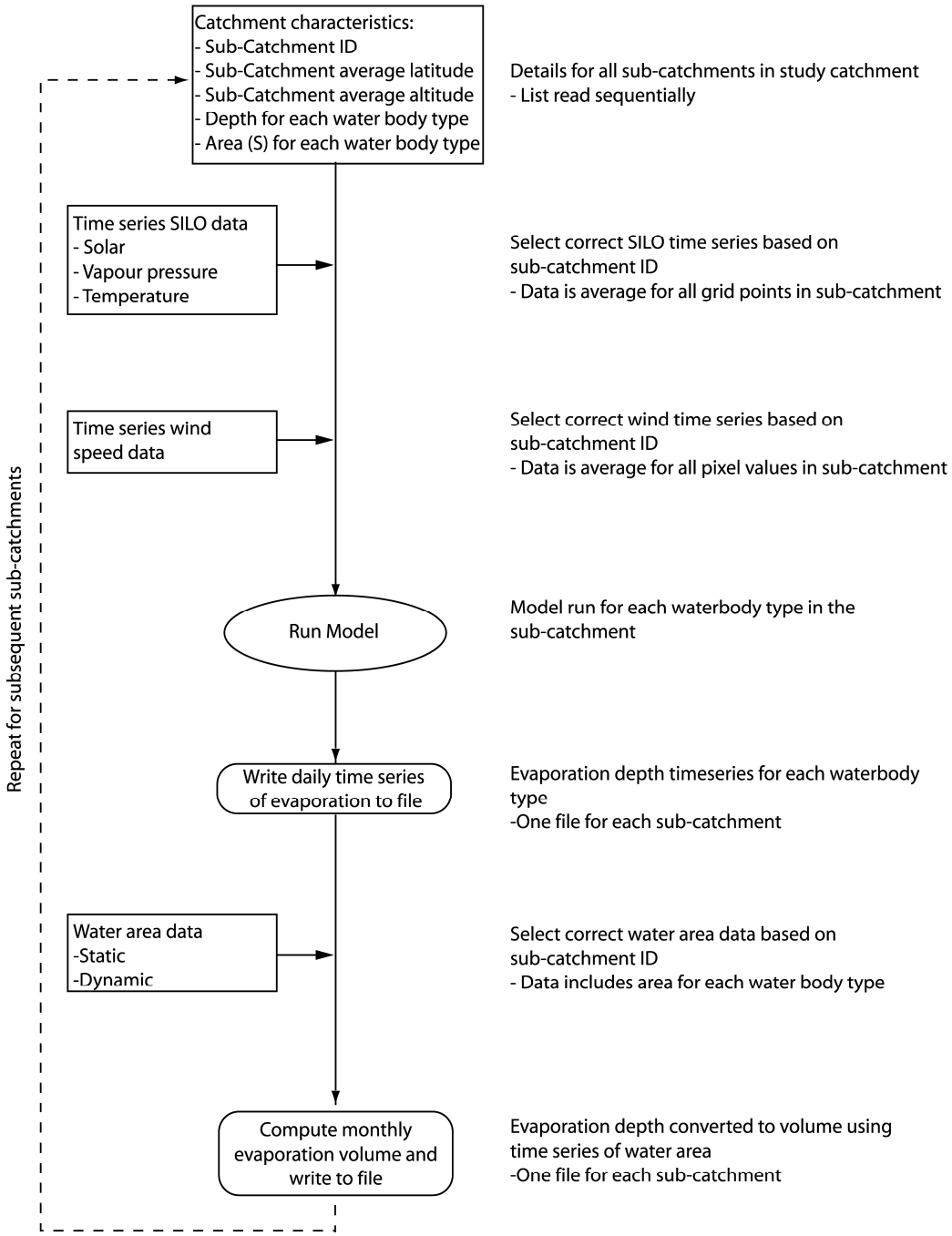

Figure 11-1. Model framework used for modelling evaporation from open water in the Murray-Darling Basin

The evaporation model was written in C# and developed using TIME. TIME is an environmental modelling framework that allows for the rapid testing and development of models using common reusable and tested components. TIME is developed on Microsoft's .NET framework. This framework and the order of file calling and writing is illustrated in Figure 11-1. A screen capture of the model running and the Paroo catchment expanded to reveal the four subcatchments within it, and the nine water body types modelled, is shown in Figure 11-2.

Figure 11-2. Open water evaporation model running with the Paroo catchment expanded to reveal the four subcatchments within it, and the nine water body types modelled

Contact Us

Phone: 1300 363 400
+61 3 9545 2176

Email: enquiries@csiro.au

Web: www.csiro.au

Your CSIRO

Australia is founding its future on science and innovation. Its national science agency, CSIRO, is a powerhouse of ideas, technologies and skills for building prosperity, growth, health and sustainability. It serves governments, industries, business and communities across the nation.